Vol. 14, No. 1 (2026), pp.21–48

CHITKARA UNIVERSITY

Journal of Pharmaceutical Technology Research and Management

Pharmacophore-Based 3D-QSAR and Molecular Docking Studies of Novel 1,3,4-Thiadiazole Derivatives as Potential α-Glucosidase Inhibitors

Debarshi Mondal[1*], Priya Devi[2*], Shalini Sharma[3] and Harmel Singh Chahal[4]

[1]*Department of Pharmaceutical Chemistry, SWIFT School of Pharmacy, Ghaggar Sarai, Rajpura, Patiala, PIN-140401, Punjab, India.*

[2]*Department of Pharmaceutical Chemistry, University School of Pharmaceutical Sciences, Rayat Bahra Professional University, Bohan, Nangal Shahidan, Hoshiarpur, PIN-146023, Punjab, India.*

[3]*Department of Pharmaceutics, SWIFT School of Pharmacy, Ghaggar Sarai, Rajpura, Patiala, PIN-140401, Punjab, India.*

[4]*Department of Pharmacology, SWIFT School of Pharmacy, Ghaggar Sarai, Rajpura, Patiala, PIN-140401, Punjab, India.*

[*]priya780780devi@gmail.com (Corresponding Author)

RESEARCH ARTICLE **Open Access**

ARTICLE INFORMATION

Received: June 28, 2026
Accepted: July 29, 2026
Published Online: August 17, 2026

Keywords:
α-Glucosidase inhibitors, 1,3,4-thiadiazole, Pharmacophore modelling, 3D-QSAR, Molecular docking

DOI: 10.15415/jptrm.2026.141002

ABSTRACT

Background: Metabolic Disorder Type 2 Diabetes mellitus (T2DM) is a chronic disease that involves hyperglycemia due to insulin resistance and impaired insulin secretion. α-glucosidase inhibition has been proven to be a therapeutic approach for controlling postprandial hyperglycemia and is a well-established treatment for T2DM. 1,3,4-thiadiazole is a promising pharmacophore among heterocyclic scaffolds due to its broad range of biological activities, including α-glucosidase inhibition.

Purpose: The present study was designed to identify and optimize novel 1,3,4-thiadiazole derivatives as α-glucosidase inhibitors using an integrated computer-aided drug design (CADD) approach that includes pharmacophore modeling, 3D-QSAR, molecular docking, optimization of R-groups, and ADMET prediction.

Methods: A total of 34 reported 1,3,4-thiadiazole derivatives were analyzed to build an optimal pharmacophore model ($AADHR_3$) as well as atom-based ($R^2 = 0.799$, $Q^2 = 0.822$) and Gaussian field-based 3D-QSAR models ($R^2 = 0.967$, $Q^2 = 0.682$). The structurally optimized lead compounds were then identified by molecular docking, R-group optimization, and ADMET prediction.

Results: The analysis of the contour map showed that bulky hydrophobic groups in the R_1 position and electron-withdrawing groups in the R_2 position were beneficial for enhancing α-glucosidase inhibitory activity. The docking score of five compounds was comparable or better than that of acarbose (−6.260 kcal/mol), with the best score being compound 25 (−6.686 kcal/mol). The designed derivatives (DM1 (−7.625 kcal/mol), DM2 (−7.418 kcal/mol), and DM3 (−7.284 kcal/mol)) showed better binding abilities and favorable interactions with Arg281, Asp282, Asp404, Asp518, Asp616, His674, and Phe525, in addition to promising ADMET properties.

Conclusion: Pharmacophore analysis, 3D-QSAR, molecular docking, SAR, and ADMET studies indicated that the 1,3,4-thiadiazole scaffold could be a promising template for designing potent α-glucosidase inhibitors. The optimized derivatives, especially DM1–DM3, are good lead candidates for further development into therapeutic drugs for T2DM.

1. Introduction

α-Glucosidase is a membrane-bound hydrolytic enzyme and is mainly found in the brush border of the small intestine; it is an essential enzyme for the digestion of carbohydrates. It is a member of the glycoside hydrolase family and performs the last step in the metabolism of carbohydrates, breaking oligosaccharides, disaccharides, and polysaccharides into absorbable monosaccharides, especially glucose (Bischoff, 1994; Chiba, 1997). After consuming a meal high in carbohydrates, the enzymes α-glucosidase, which include maltase, sucrase, and isomaltase, break down complex carbohydrates into glucose that is then absorbed into the bloodstream. This process is an important cause of increased blood glucose after a meal, a key pathological process in type 2 diabetes

mellitus (T2DM) (Van de Laar *et al.,* 2005). Under normal physiological conditions, after eating a meal, the amount of glucose in the blood rises quickly, which triggers the pancreatic beta cells to secrete insulin and thus keep the blood glucose level in control. In patients with T2DM, however, inadequate insulin secretion and insulin resistance render the utilization of glucose inadequate, leading to chronic hyperglycemia and its associated complications. Thus, α-glucosidase has come into the spotlight as a drug target for postprandial hyperglycemia (Figure 1) (Hanefeld, 2007). Acarbose, miglitol, and voglibose (Figure 2) are clinically approved α-glucosidase inhibitors used in combination with other antidiabetic drugs or as monotherapy. The drugs act locally within the gastrointestinal tract with low to negligible systemic absorption and thus have a good safety profile (Van de Laar *et al.,* 2005). The structure of α-glucosidase is such that it contains several conserved amino acid residues that are crucial for recognizing the substrate and catalyzing hydrolysis. In mammalian and microbial α-glucosidases, the following residues are found to be important catalytic residues involved in proton transfer and glycosidic bond cleavage: Asp518, Glu616, His674, and Arg600. Carbohydrate substrates bind to the active site with hydrogen, hydrophobic, and van der Waals interactions with multiple subsites in the active site. These catalytic residues are highly reactive with effective α-glucosidase inhibitors, which block binding of the substrate and the enzyme activity (Shen *et al.,* 2015). Over the past few years, there has been a great deal of research on the synthesis of new α-glucosidase inhibitors derived from synthetic heterocyclic compounds, natural products, flavonoids, alkaloids, terpenoids, and peptidomimetic derivatives. It has been observed that heterocycles like triazoles, pyrazoles, thiazoles, quinazolines, indoles, and triazolopyrazines show promising α-glucosidase inhibitory activity and can be considered as promising leads for the development of antidiabetic drugs (Patel, 2024).

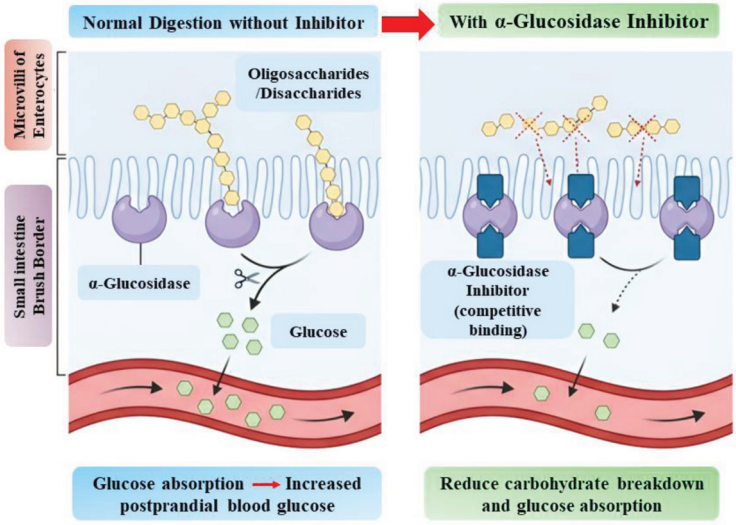

Figure 1: Mechanism of Action of α-Glucosidase

The 1,3,4-thiadiazole ring system represents one of the most important and versatile heterocyclic moieties in medicinal chemistry, which exhibits various biological activities, including anticancer, antimicrobial, antitubercular, antifungal, anti-inflammatory, antiviral, anticonvulsant, antioxidant, and antidiabetic activities (Hu *et al.,* 2014; Jain *et al.,* 2013; Uddin, 2023; Matysiak *et al.,* 2015; Dawood & Farghaly, 2017). The scaffold comprises a 5-membered aromatic ring containing 2-N atoms and a single S atom, providing unique electronic properties to its highly interesting pharmacological properties. The 1,3,4-thiadiazole ring is also a significant bioisostere of pyrimidine, oxadiazole, thiazole, and ester structures and has other desirable properties, such as aromaticity, electron deficiency, and structural rigidity, that enhance the pharmacokinetic and pharmacodynamic properties of drug candidates. The planar structure and the high resonance stabilization of the 1,3,4-thiadiazole ring make this molecule able to interact efficiently with biological macromolecules. The electronegative atoms such as N and S can form strong hydrogen bonding, dipole-dipole, and π-π interactions with active sites of enzymes or pockets of receptors. Substitutions at the 2nd and 5th positions, which are the places where the heteroatoms are located, can have a significant impact on the lipophilicity, metabolic stability, target selectivity, and biological activity of the molecule. Thiadiazole derivatives have been proven to inhibit enzymes such as α-glucosidase, carbonic

anhydrase, cyclooxygenase (COX), tyrosine kinases, histone deacetylases, and dipeptidyl peptidase-4 (DPP-4). The scaffold has also been shown to be active against the signaling pathways involved in cancer by modulation of protein kinases and the promotion of cell death (apoptosis) in tumor cells. Additionally, its sulfur-aromatic backbone also increases its permeability through the membrane and binding affinity to hydrophobic areas in biological targets. This 1,3,4-thiadiazole scaffold is also very modulable, where a large number of structural modifications can be performed without loss of biological activity. Other functionalization sites on the ring allow researchers in medicinal chemistry to alter the pharmacological properties, enhance oral bioavailability, reduce toxicity, and boost metabolic stability. Therefore, the 1,3,4-thiadiazole family has emerged as a privileged structural moiety in modern medicinal chemistry and remains an important part of drug development and the treatment of cancer, infectious diseases, inflammation, neurological diseases, and diabetes mellitus. The success of many thiadiazole derivatives in preclinical and clinical studies underlines the great prospect of this scaffold for drug discovery and development.

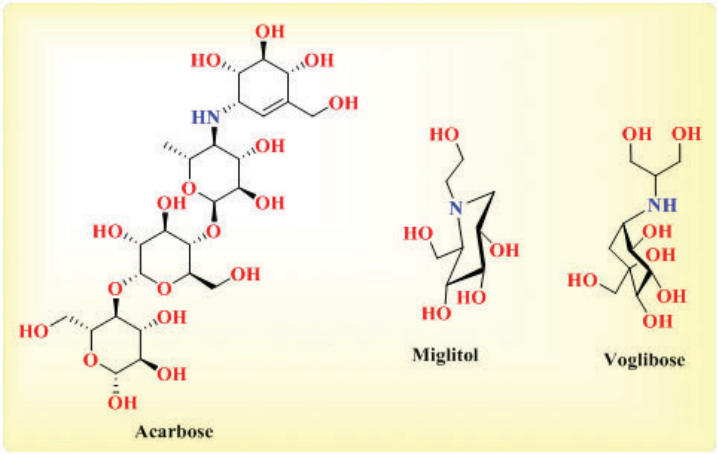

Figure 2: Schematic Representation of Drugs of the α-Glucosidase Inhibitor

The present work aimed to develop structure-based, alignment-dependent 3D-QSAR models which were then used in conjunction with both atom-based and field-based analysis to investigate the structure-activity relationship of a wide variety of 1,3,4-thiadiazole-based α-glucosidase inhibitors (Figure 3). Based on the main structural attributes of these compounds, a five-point pharmacophore hypothesis was drawn up. The most favourable conformations of the dataset molecules were determined, and then, 3D-QSAR modelling was carried out by the molecular docking process. Docking was also performed for an insight into the binding affinity and interaction of the ligands with the α-glucosidase. The best QSAR model was chosen from the generated QSAR models using several statistical validation criteria, such as standard deviation (SD), non-cross-validated R2, R2 scramble, leave-one-out (LOO) cross-validation Q2, F-test value, p-value, and root mean square deviation (RMSD). The 3D contour maps derived from the atom-based and field-based analyses were employed to find the important pharmacophoric features that could be exploited for the development of potent and selective α-glucosidase inhibitors. This refined pharmacophore model can provide an efficient tool towards the development of new compounds, such as improved α-glucosidase, which could result in better management of type 2 diabetes. The 34 analogues of 1,3,4-thiadiazole were subjected to computational analysis, which was confirmed by the literature. A three-dimensional (3D) pharmacophore mapping was done to determine the structural requirements for biological activity. While pharmacophore modelling, 3D-QSAR, molecular docking, virtual screening and ADMET prediction in themselves are well-documented computational approaches, their systematic combination in a single computer-aided drug design workflow specifically to optimise 1,3,4-thiadiazole-based α-glucosidase inhibitors is novel. The validated pharmacophore model was combined with the complementary atom-based and Gaussian field-based 3D-QSAR methodologies for defining the key structural factors that influence inhibitory activity, rather than being used alone. This was followed by rational optimisation of the R-group, virtual screening of an enumerated library of 1,419 derivatives, docking-based prioritisation and ADMET filtering to provide three structurally optimised lead candidates (DM01, DM02, and DM03). The novelty of the present study lies in the development of an integrated structure-guided optimisation strategy that enables translation of SAR information into rational lead design and gives practical guidelines for molecular design of future α-glucosidase inhibitors.

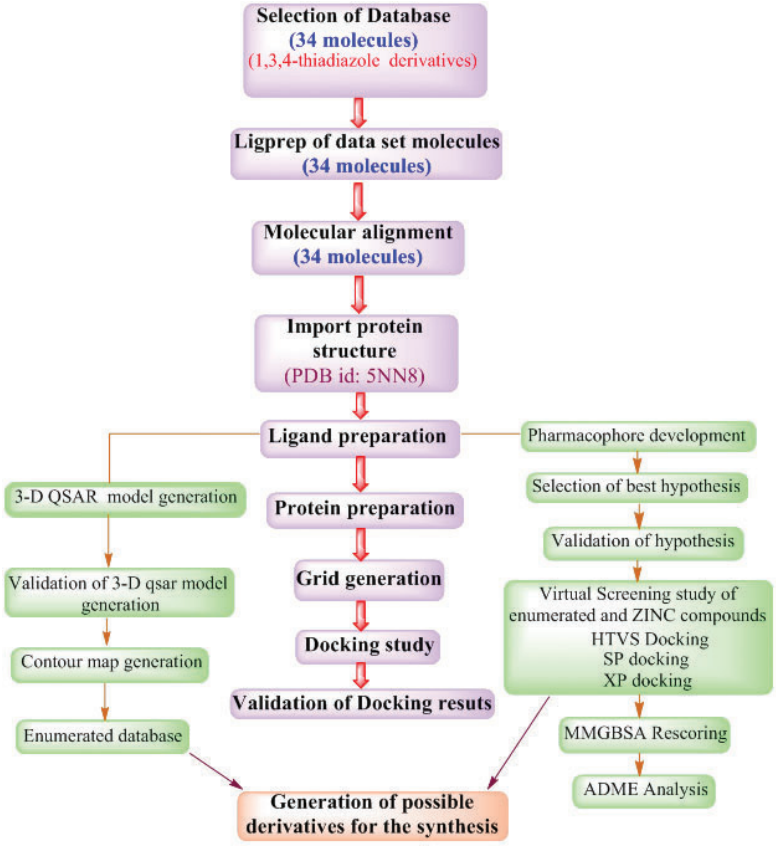

Figure 3: Workflow Describing the Computational Methods for the Discovery of Potential α-Glucosidase Inhibitors

2. Materials and methods

2.1. Selection of the Data Set and Preparation of Ligands

A set of 34 previously reported α-glucosidase inhibitory 1,3,4-thiadiazole derivatives was used to investigate the α-glucosidase inhibitory activity. Although the dataset size is modest, it represents a chemically homogeneous congeneric series and was generally considered suitable for ligand-based 3D-QSAR modelling, as the structural alignment and consistency of biological endpoints enhance the interpretability of the model. To prevent possible model overfitting, the dataset was randomly split into an independent training set and test set, and the models built were tested with various internal and external validation statistics, such as R^2, Q^2, R^2CV, $R^2Scramble$, Pearson correlation coefficient, RMSE, F-test, p-value and external predictive statistics. Thus, even with the small number of compounds applied, reasonable confidence in the robustness and predictive performance of the models in the defined chemical space can be obtained from the applied validation procedures. The chemical structures were first acquired in two-dimensional (2D) format from the published data and then drawn using ChemDraw Professional 16.0 (Cambridge, MA, USA). The 2D structures were then energy-optimised to 3D structures for computational analysis. The reported IC_{50} values (3.460-6.251 μM) were converted to quantitative structure-activity relationship (QSAR) modelling using the corresponding pIC_{50} values (Akdağ *et al.,* 2025; Kaya *et al.,* 2025; Kaya *et al.,* 2024; Shulgau *et al.,* 2024). The structures of all the compounds are based on a 1,3,4-thiadiazole scaffold; their substituents are shown in Table 1, and the experimental IC_{50} and calculated pIC_{50} values are also presented. The data set was randomly split into an 80% training set and a 20% test set to build the 3D-QSAR models. Five partial least squares (PLS) components were used for model generation, based on the pharmacophore hypothesis selected. Before the model building, all molecules were energy minimised, and then the molecules were put on a common molecular framework to ensure a common orientation in space for the molecules, allowing for reliable QSAR analysis, as shown in Figure 4.

2.2. Alignment of the Dataset

Structural alignment is an important requirement for the creation of reliable molecular field descriptors and for the

establishment of a good 3D-QSAR model. If the molecules are properly aligned, they all have the same orientation in three-dimensional space with the same spatial structure, which enhances the relationship between structure and bioactivity. On the contrary, if the molecules are not aligned properly, the predictive accuracy and reliability of the resultant QSAR model will be reduced. The present study used an automatic reference option in Maestro version 12.5 that utilizes a flexible ligand alignment to create an optimal common orientation of the dataset compounds. All the compounds in the dataset were aligned to a single optimal alignment hypothesis and subsequently used for the 3D-QSAR model development as indicated in Table 1 and Figure 4.

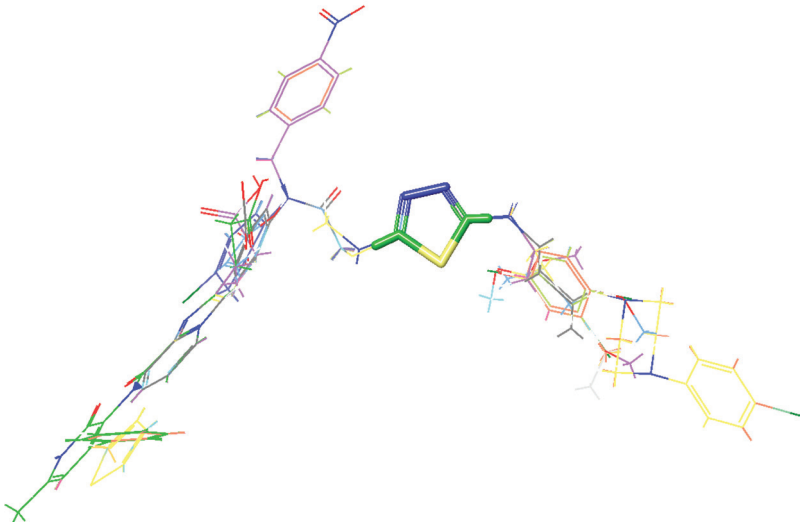

Figure 4: Alignment of Dataset Molecules

Table 1: Description of Substitutions on the Core Moiety with IC50 and pIC50 Values

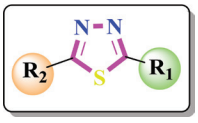

Comp.	R1	R2	IC_{50} (µm)	pIC_{50} (µm)
01		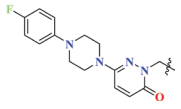	0.561	6.251
02		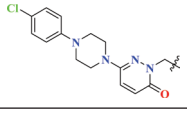	1.203	5.920
03		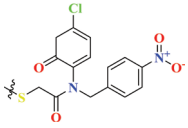	12.58	4.900
04		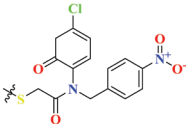	99.01	4.004

05		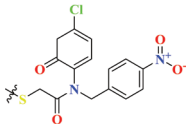	346.51	3.460
06		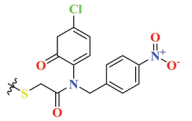	12.16	4.915
07	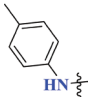	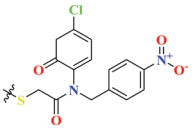	4.68	5.330
08	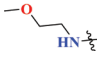	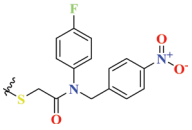	16.51	4.782
09		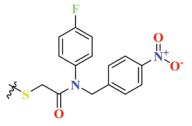	34.65	4.460
10		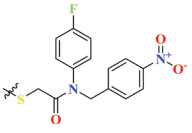	8.25	5.084
11	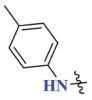	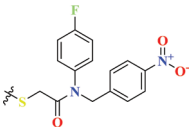	8.15	5.089
12		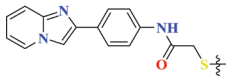	33.04	4.481
13		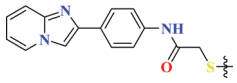	6.09	5.215
14		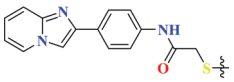	77.5	4.111
15		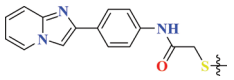	88.65	4.052
16		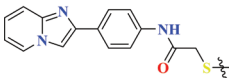	13.03	4.885
17		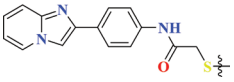	31.15	4.507

18		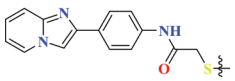	38.03	4.420
19		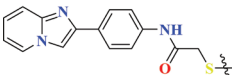	43.4	4.363
20		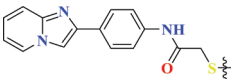	15.68	4.805
21		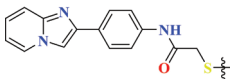	119.8	3.922
22		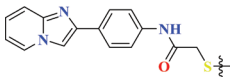	48.87	4.311
23		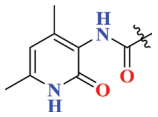	16.22	4.790
24		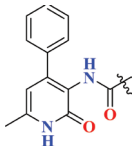	10.22	4.991
25		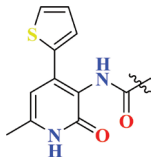	18.58	4.731
26		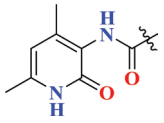	20.83	4.681
27		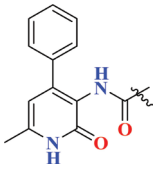	6.7	5.174
28		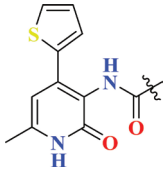	8.42	5.075
29		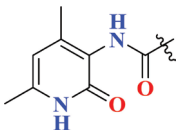	17.93	4.746

30		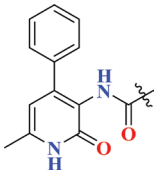	10.36	4.985
31		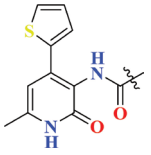	48	4.319
32	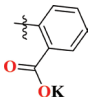	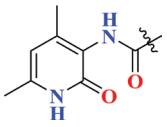	14.02	4.853
33	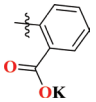	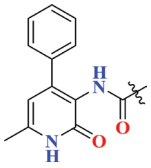	3.66	5.437
34	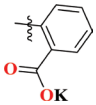	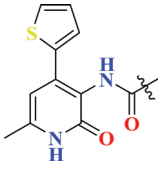	24.51	4.611

2.3. Transformation of IC50 and Selection of Test and Training Set

The biological activity of the set of compounds is expressed in IC_{50} values (μM). The experimental IC_{50} values were converted to their respective pIC_{50} values using the Calculator module in Schrödinger Maestro version 12.5 and the following equation: $pIC_{50} = -\log_{10}(IC_{50})$. The values of pIC_{50} obtained were used as the dependent variable for 3D-QSAR model development. All calculated pIC_{50} values were lowered by 6 to prevent negative activity values while generating the model. All the molecular alignment sets were randomly split into training and test sets as summarized in Table 1 to build and test the predictive ability of QSAR models. The dataset was randomly divided into training (80%) and test (20%) subsets to ensure that the test compounds remained completely independent during model development. Random splitting was selected because the dataset represents a structurally homogeneous congeneric series sharing a common 1,3,4-thiadiazole scaffold and comparable biological assay conditions, thereby minimizing structural heterogeneity between the subsets. Furthermore, the predictive performance of the developed models was evaluated using both internal cross-validation and an independent test set, allowing assessment of model robustness while reducing the possibility of biased model fitting.

2.4. Generation of 3D-QSAR Model

The aligned dataset (Table 2) was used to generate the atom-based and Gaussian field-based 3D-QSAR models independently in Maestro version 12.5. For the atom-based 3D-QSAR model, the grid spacing was set to be 1.0 Å, and the molecular grid was expanded 3.0 Å beyond the training set. Within 2.0 Å of any atom in the training set, force-field contributions were ignored, and the steric and electrostatic energy values were cut off at 30.0 kcal/mol. Insignificant variables were removed with a standard deviation (SD) less than 0.01. Model validation was carried out by the leave-one-out (LOO) cross-validation method. The number of partial least squares (PLS) factors used was set to 4 for both atom-based and Gaussian field-based 3D-QSAR models. The atom-based model included hydrogen bond donor (HBD), hydrophobic, and electron-withdrawing descriptors, while the Gaussian field-based model was built to derive reliable relationships between molecular descriptors and α-glucosidase inhibitory activity based on steric, electrostatic, hydrogen bond acceptor (HBA), and hydrogen bond donor (HBD) field descriptors (Bisht *et al.,* 2025; Verma *et al.,* 2021; Vishwakarma & Bhatt, 2021).

Table 2: Generation of 3D-QSAR Model Actual pIC_{50}, Predicted pIC_{50} and Residual Values

Comp. No.	Actual pIC_{50} (x)	Atom based		Field based	
		Predicted pIC_{50}	Residuals	Predicted pIC_{50}	Residuals
		(Ÿ)	(Ÿ -X)	(Ÿ)	(Ÿ -X)
1*#	6.251	5.839	-0.412	5.971	-0.280
2	5.920	5.877	-0.043	6.001	0.081
3	4.900	4.482	-0.418	4.853	-0.047
4	4.004	4.249	0.245	4.115	0.111
5	3.460	3.934	0.474	3.460	0.040
6	4.915	4.708	-0.207	4.896	-0.019
7	5.330	5.048	-0.282	5.340	0.010
8	4.782	4.828	0.046	4.803	0.021
9	4.460	4.321	-0.139	4.465	0.005
10	5.084	5.113	0.029	5.067	-0.017
11	5.089	5.403	0.314	5.068	-0.021
12*#	4.481	4.446	-0.035	4.644	0.163
13	5.215	4.908	-0.307	5.299	0.084
14	4.111	3.680	-0.431	4.102	-0.009
15*#	4.052	4.210	0.158	4.883	0.831
16	4.885	4.730	-0.155	4.682	-0.203
17	4.507	4.627	0.120	4.646	0.139
18	4.420	4.398	-0.022	4.353	-0.067
19	4.363	4.538	0.175	4.377	0.014
20*#	4.805	4.432	-0.373	4.500	-0.305
21	3.922	4.258	0.336	3.939	0.017
22	4.311	4.531	0.220	4.310	-0.001
23	4.790	4.768	-0.022	4.774	-0.016
24*#	4.991	5.175	0.184	4.977	-0.014
25	4.731	4.730	-0.001	4.791	0.060
26	4.681	4.846	0.165	4.787	0.106
27	5.174	5.255	0.081	5.070	-0.104
28	5.075	4.813	-0.262	4.922	-0.153
29	4.746	4.530	-0.216	4.555	-0.191
30	4.985	4.930	-0.055	4.981	-0.004
31	4.319	4.491	0.172	4.462	0.143
32	4.853	5.032	0.179	5.016	0.163
33	5.437	5.441	0.004	5.335	-0.102
34*#	4.611	4.973	0.362	4.687	0.076

Note: Compounds marked with an asterisk (*) represent the test set used for validation of the atom-based 3D-QSAR model, whereas compounds marked with a hash symbol (#) represent the test set used for validation of the Gaussian field-based 3D-QSAR model.

2.4.1. Partial Least Squares (PLS)/3D-QSAR Model Evaluation of Atom-based and Field-based

Partial least squares (PLS) regression analysis was used to develop the relationship between the pIC_{50} values (dependent variable) and the associated molecular field descriptors (independent variable) for the atom-based 3D-QSAR and for the Gaussian field-based 3D-QSAR model. Several parameters were employed for assessing the predictive performance and statistical reliability of the models obtained by QSAR, such as non-cross-validated coefficient (R^2), cross-validated coefficient (Q^2), leave-one-out (LOO) cross-validation, R^2 scramble, cross-validated R^2CV, F-test, root mean square error (RMSE), p-value, Pearson correlation coefficient (Pearson-r), and standard deviation (SD) (Table 3). The following validation criteria were defined for a statistically reliable QSAR model: RMSE near zero, SD < 0.5, R^2 between 0.6 and 1.0, $Q^2 > 0.5$, and the difference of $R^2 - Q^2 < 0.3$. Further, a high F-value along with a low p-value showed high statistical significance and proved the strength and predictive power of the developed QSAR models (Bisht *et al.*, 2025; Gholami Rostami & Fatemi, 2018; Gholami Rostami & Fatemi, 2019; Singh *et al.,* 2022).

Table 3: Pharmacophore Hypothesis Development with Scores and their Ranking

PLS Statistics	Reference values	Atom based	Gaussian field based
SD	SD of regression < SD of actual activities	0.249	0.102
R^2	> 0.6	0.799	0.967
R^2_{CV}	> 0.5	0.713	0.631
$R^2_{Scramble}$	> 0.5	0.598	0.886
F	Larger values of F	122.9	166.2

P	The less the values of P, the greater the degree of confidence	9.61e-08	1.29e-16
RMSE	Close to 0	0.29	0.39
Q^2	> 0.5, and (R^2 - Q^2) < 0.3	0.822	0.682
Pearson-r	Close to 1, lesser scattered predictive activities in the plot of observed *Vs.* predicted activities	0.913	0.845

2.4.2. Contour Map Generation

The influence of various molecular features around the 1,3,4-thiadiazole scaffold on the predicted α-glucosidase inhibitory activity was analysed using contour mapping. Using contour map visualisation, the influence of various molecular descriptors around the 1,3,4-thiadiazole skeleton on the predicted α-glucosidase inhibitory activity was analysed. The 3D-QSAR models were built either by atoms or by Gaussian fields, and both models can generate contour maps that represent regions likely to have a significant impact on biological activity based on the presence of a specific molecular property, such as hydrogen bond donor, hydrogen bond acceptor, hydrophobic, steric, or electron-withdrawing. Positive contour coefficients mean the spatial position is favourable for the introduction of the molecular feature, while negative values denote unfavourable regions for the introduction of the molecular feature. Each molecular descriptor is shown in its own colour scheme; hence, the colour for a region with a favourable molecular descriptor is different in each molecular descriptor contour map and must be interpreted individually for that molecular descriptor in the following sections (Bisht *et al.,* 2025).

2.4.3. External Validation of 3D-QSAR Model

The developed 3D-QSAR model was also externally validated using an independent and structurally diverse test set to assess its predictive ability. The finalised model was applied to predict the biological activity of the test compounds, and the predicted pIC_{50} values were correlated with the experimental ones to check the robustness and prediction accuracy of the model. Several statistical parameters were used for external validation, such as the predictive correlation coefficient (r^2pred), the slopes of the regression lines (k and k′), the coefficients of determination through the origin (R_0^2 and $R'_0{}^2$), and the modified squared correlation coefficients [r^2m (LOO), r^2m, and r'^2m]. These validation parameters were used as criteria to establish good external predictive ability in a QSAR model. A predictive correlation coefficient (r^2pred) > 0.6 was obtained, which showed that the developed model was statistically sound, reliable, and had a good predictive capability for the α-glucosidase inhibitory activity of structurally diverse 1,3,4-thiadiazole derivatives (Asati *et al.*, 2017; Veerasamy *et al.*, 2011).

- $\left(r^2 - R_0^2\right)/r^2 < 0.1, \left(r^2 - r_0'^2\right)/r^2 < 0.1.$
- $0.85 < K < 1.15 \, or \, 0.85 < K' < 1.15.$
- $r^2 m < 0.5.$

2.5. Pharmacophore Development

The pharmacophore modelling was carried out to determine the important functional groups contributing to the α-glucosidase inhibitory activity. The pharmacophore hypothesis was derived from the correlation of the structural features of the compounds with their respective pIC_{50} values from the available report. The PHASE module in Schrödinger Maestro version 12.5 was used for the pharmacophore generation. The compounds were grouped according to their biological activities into active (10-15%), inactive (25-30%) and intermediate. The pharmacophore search was performed with the default parameters of the software (box size 1 Å, minimum inter-site distance 2 Å). The following pharmacophoric features were selected: aromatic rings (R), hydrogen bond acceptors (A), hydrogen bond donors (D), hydrophobic groups (H) and positively or negatively charged ionisable groups. In total, 20 pharmacophore hypotheses have been created, with the best model being found as AADHR_3. The optimised AADHR_3 pharmacophore hypothesis, which represents the necessary molecular features for α-glucosidase inhibition, is shown in Figure 5**.** Two hydrogen bond acceptors and one hydrogen bond donor, one hydrophobic feature and one aromatic ring were used in the structural framework to perform molecular alignment and development of 3D-QSAR models. These pharmacophoric properties were also used as the primary design criteria during R-group optimisation to ensure that the new derivatives had the same interaction that led to biological activity. Representative compounds from each activity class (active (33, 01, 02), inactive (22, 04, 05, 18, 21) and intermediate (19)) were used in the construction of the pharmacophore model. These hypotheses were then assessed using several scoring criteria, including survival score, site score, vector alignment, volume overlap, and inactive match, along with receiver operating characteristic (ROC) analysis, to identify the best and most predictive pharmacophore model for 3D-QSAR analysis (Bisht *et al.,* 2025; Vanajothi *et al.,* 2020).

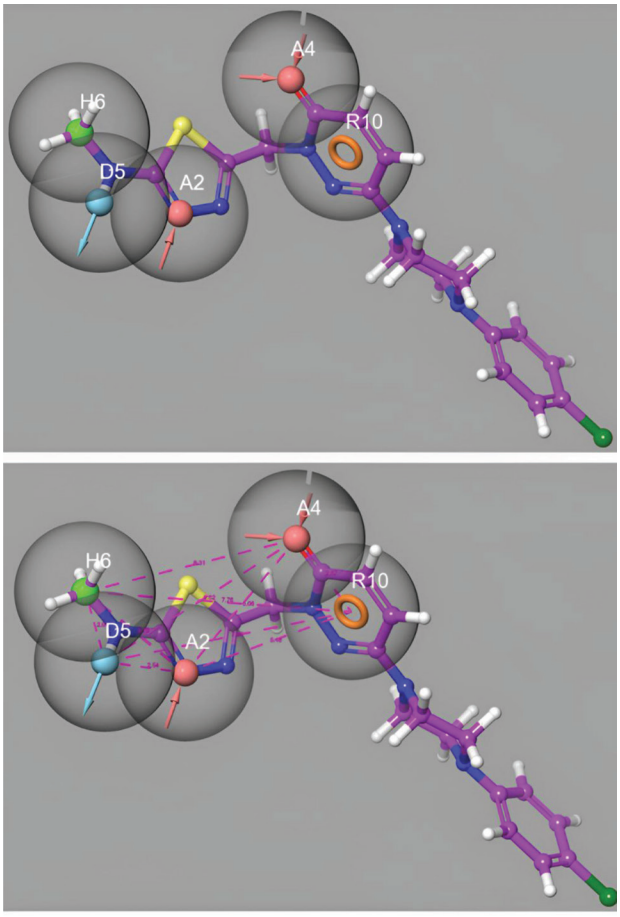

Figure 5: Best Pharmacophoric Hypothesis AADHR_3

2.6. R-group Enumeration for New Compounds Generation

The design of R-group substituents was based on the combined analysis of pharmacophore mapping, 3D-QSAR contour maps based on both atoms and Gaussian fields, and structure-activity relationship (SAR) studies of α-glucosidase inhibitors published in the literature. The contour maps revealed spatial areas that were conducive to the presence of hydrophobic, hydrogen-bond donor, hydrogen-bond acceptor, steric, and electron-withdrawing substituents, while the docking analysis represented interactions of the substituents with the catalytic residues Arg281, Asp282, Asp518, Asp616, Arg600, and His674 that were conserved across the entire structure. Therefore, a wide range of synthetically accessible groups with hydrophobic, aromatic, electron-withdrawing, and hydrogen-bond-donating properties were chosen to enable the possibility of achieving the most favorable ligand-protein interactions while still maintaining the structural integrity of the 1,3,4-thiadiazole ring system. The method of R-group enumeration was used to systematically replace the substituent groups on the parent scaffold by chemically relevant functional groups, thus generating structurally diverse derivatives of the 1,3,4-thiadiazole. The 3D-QSAR model was used as a template for the structure design of these new analogs, through which favorable substitution sites were found and the physicochemical characteristics that were required for the enhancement of biological activity were determined. The core structure of 1,3,4-thiadiazole was kept unchanged during the design process. The contour map analysis led to the introduction of different R1 substituents to fine-tune the interactions within the binding pocket, and appropriate R2 substituents were added for enhancing the molecular properties such as solubility and receptor binding (Figure 6). The chosen substituents were carefully chosen to achieve appropriate hydrogen-bonding donor and acceptor functionality to enable favorable interactions with the target enzyme. With this approach, a library of 1,419 R-group-enumerated derivatives was generated and then virtually screened using the Schrödinger Suite (Schrödinger LLC, New York, NY, USA) to find potential compounds with higher α-glucosidase inhibitory activity (Gupta *et al.,* 2025; Sharma *et al.,* 2025; Polya *et al.,* 2012).

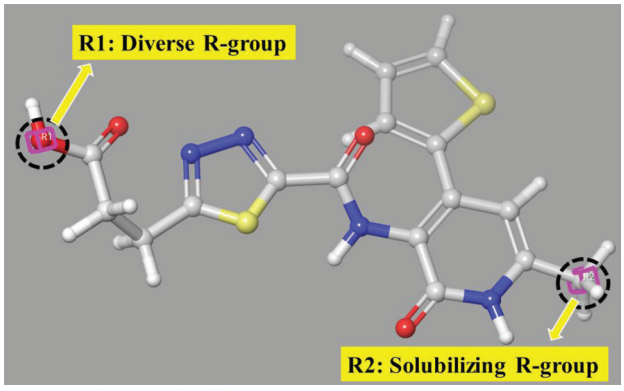

Figure 6: Substitution of R-position Enumeration for New Compounds Generation

2.7. Virtual Screening of R-Group-Enumerated Compound Generation

A library of 1,419 R-group-enumerated 1,3,4-thiadiazole derivatives was created and screened virtually for finding potential lead compounds having enhanced α-glucosidase inhibitory activity. All enumerated molecules were submitted to the Schrödinger Maestro 12.5 software, where their three-dimensional models were created and energy minimized using the OPLS4 force field before screening. This optimized compound library was then processed for a hierarchical molecular docking with the Glide module. The

docking protocol was tested with the compound used as a reference, 2-((2-(dimethylammonio)ethyl)amino)-5-(5-(2-(methylammonio) ethyl)-1,3,4-thiadiazole-2-carboxamido)-6-oxo-4-(thiophen-2-yl)-3,6-dihydropyridin-1-ium-3-ide. All compounds were initially docked with the active site of the α-glucosidase in the HTVS mode, with flexible ligand docking, to quickly identify candidate compounds. The best molecules identified by HTVS were redocked with the Standard Precision (SP) protocol to enhance the accuracy of docking. Lastly, the most successful compounds at the SP stage were further docked with the Extra Precision (XP) docking protocol to get very reliable binding poses and docking scores. The selected compounds were then evaluated by the validated 3D-QSAR model to predict their biological activity and pinpoint the potential promising compounds as lead compounds for optimization.

2.8. Molecular Docking

To explore the binding interactions of the 1,3,4-thiadiazole derivatives with α-glucosidase, molecular docking studies were carried out using the Glide module of Schrödinger Maestro version 12.5. The crystal structure of α-glucosidase (PDB ID: 5NN8; resolution: 2.45 Å) was retrieved from the RCSB Protein Data Bank and was prepared by adding hydrogen atoms, assigning bond order, removing crystallographic water molecules, and energy minimizing the protein using the OPLS4 force field with the Protein Preparation Wizard. A receptor grid of 20 × 20 × 20 Å was generated by centering it on the co-crystallized ligand with the coordinates X = -13.97, Y = -38.18, and Z = 95.19. Ligand structures were rendered using the LigPrep module to obtain low-energy 3D conformations before docking was performed. Molecular docking was then performed with the Extra Precision (XP) protocol with no positional preference in the ligand, and blind docking was used to investigate possible binding sites throughout the surface of the protein. The protein-ligand complexes were then analyzed on XP Visualizer to find important interactions between protein and ligand (Yadav *et al.,* 2021; Cevik *et al.,* 2023; Vishwakarma & Bhatt, 2021; Stitou *et al.*, 2021).

2.8.1. Validation of the Molecular Docking Protocol

The co-crystallized ligand (acarbose) from the crystal structure of α-glucosidase (PDB ID: 5NN8) was extracted and prepared in the same manner as the dataset compounds and re-docked into the prepared receptor using the Glide XP docking protocol for validation of the molecular docking protocol. The docking accuracy was assessed using the root-mean-square deviation (RMSD) between the docking and crystallographic pose of the ligand based on heavy atoms. The RMSD value below 2.0 Å has been regarded as a good indicator of successful production of the experimentally observed binding mode, which suggests that the docking protocol was adaptable for predicting the binding orientations of ligands (Figure 7) (Vishwakarma & Bhatt, 2021; Stitou *et al.*, 2021).

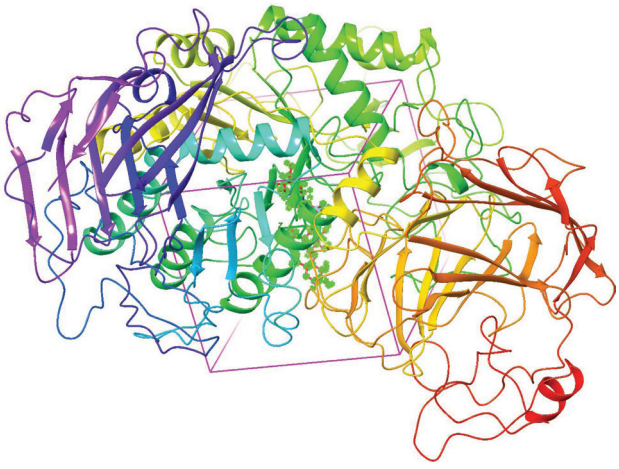

Figure 7: Generated Grid within the α-Glucosidase, Co-crystallised Acarbose (Red), and Redocked Acarbose (green)

2.9. ADME Prediction

The Schrödinger Maestro version 12.5 software with the QikProp module was used for the prediction of absorption, distribution, metabolism, and excretion properties of the selected compounds (Hosen *et al.,* 2017). The compounds were assessed for druglike properties by several important pharmacokinetic descriptors such as molecular weight, hydrogen bond donors and acceptors, dipole moment, rotatable bonds, and the predicted human oral absorption (HOA). Other physicochemical parameters, including aqueous solubility (QPlogS) and skin permeability (QPlogKp), were also predicted, which helps to estimate their pharmacokinetic behavior (Inamdar *et al.,* 2023). Moreover, the drug likeness of the compounds was assessed based on Lipinski's Rule of Five, which focuses on various molecular properties like molecular weight, number of hydrogen bond donors, etc. (Haritha *et al.,* 2024).

3. Results and Discussion

3.1. Data Set of Top Pharmacophore Hypotheses

Twenty pharmacophore hypotheses were created representing the key molecular features for α-glucosidase inhibitory activity. Table 4 shows the systematic evaluation of the hypotheses generated by the pharmacophore. Here,

the hypothesis AADHR_3 was chosen as the best hypothesis to build a reliable structural template for subsequent QSAR modeling and virtual screening, which laid the foundation of the complete computational workflow. Of these, the most reliable pharmacophore hypothesis AADHR_3, which shows the best correlation between the pharmacophoric features and the biological activity, survived with a survival score and a hypothesis pose score (Figure 5). In addition, the Distance Computation tool was used to compute the spatial arrangement and inter-feature distances of the chosen AADHR_3 pharmacophore model. The computed distance map (shown in Table 5) gives the geometric relationship between the various pharmacophoric features, and it also gives a structural framework for molecular alignment and development of the 3D-QSAR model. These spatial relationships were useful for the subsequent 3D-QSAR analyses and helped in the rational placement of new substituents in the course of lead optimization.

Table 4: Pharmacophore Hypothesis Development with Scores and their Ranking

HypoID	Survival	Site	Vector	Volume	Select	Matches	Inactive	Adjusted	BEDROC	RefLig
AAHRR_1	4.6318	0.6803	0.7788	0.7541	1.9414	3	1.2739	3.3579	0.975	mol_17
ADHRR_1	4.5278	0.6084	0.9174	0.6832	1.8416	3	1.2846	3.2432	0.9935	mol_20
ADHRR_2	4.5186	0.558	0.9555	0.6355	1.8925	3	1.3208	3.1978	0.9574	mol_20
ADHRR_3	4.4949	0.6035	0.9224	0.6439	1.848	3	1.3172	3.1778	0.8678	mol_20
AADHR_1	4.3843	0.6339	0.9311	0.6359	1.7063	3	1.3513	3.033	1	mol_20
AADHR_2	4.3086	0.6445	0.9169	0.6367	1.6334	3	1.1703	3.1383	0.9409	mol_20
AADHR_3	4.3053	0.6828	0.9015	0.6551	1.5888	3	1.069	3.2364	0.969	mol_20
AADHR_4	4.2887	0.6579	0.9163	0.6288	1.6085	3	1.1594	3.1293	0.8882	mol_20
AADHR_5	4.2725	0.6431	0.9366	0.6667	1.549	3	1.1228	3.1497	1	mol_20
AADHR_6	4.1984	0.6017	0.8979	0.613	1.6087	3	0.886	3.3124	0.8175	mol_17
AHRR_1	4.5128	0.8111	0.9364	0.7617	1.5264	3	1.3589	3.1539	0.9872	mol_17
AHRR_2	4.3185	0.7319	0.9547	0.6891	1.4658	3	1.1165	3.202	0.975	mol_17
AHRR_3	4.2779	0.5928	0.9389	0.7395	1.5296	3	1.2529	3.0249	0.8065	mol_17
DHRR_1	4.2725	0.6823	0.9669	0.6623	1.484	3	1.5088	2.7638	0.9574	mol_20
ADHR_1	4.2009	0.709	0.9747	0.6452	1.3948	3	1.5568	2.6441	0.9632	mol_20
DHRR_2	4.1628	0.6271	0.929	0.646	1.4836	3	1.3786	2.7841	0.7938	mol_20
ADHR_2	4.1284	0.799	0.9535	0.6592	1.2396	3	1.2164	2.912	1	mol_20
AHRR_4	4.102	0.6022	0.9554	0.6709	1.3964	3	1.3364	2.7656	0.6746	mol_20
ADHR_3	4.0731	0.7044	0.8883	0.6375	1.3658	3	1.4701	2.603	0.884	mol_20
ADHR_4	4.0649	0.7189	0.9468	0.6459	1.2761	3	1.2696	2.7952	0.9254	mol_20

Table 5: Distance Mapping of Best Pharmacophoric Hypothesis AADHR_3

AADHR_3	Features Type	X	Y	Z
A2	H- bend acceptor	3.88	-3.43	1.54
A4	H- bend acceptor	1.07	-4.18	-2.61
D5	H- bend donor	4.89	-5.48	2.64
H6	Hydrophobic	5.28	-6.94	1.21
R10	Aromatic ring	0.12	-1.89	-1.64

3.2. Validation of Pharmacophore Model

Additionally, receiver operating characteristic (ROC) and percentage screen analyses were used to further assess the predictive power of the selected pharmacophore hypothesis. While the percentage screen plot shows how well the pharmacophore model was able to retrieve the active compounds from the overall set of compounds, the ROC curve demonstrates the relationship between the sensitivity and specificity of the model at various

classification thresholds. The ideal pharmacophore model would be one where all compounds were separated completely, which would yield an ROC curve that passes through the upper left corner, with 100% sensitivity and 100% specificity. The AUC and ROC values of the selected pharmacophore hypothesis (AADHR_3), as shown in Figure 8, were very good, with the values 1.00 and 1.00, respectively, which indicated that the hypothesis was very efficient to classify the compounds as active or inactive. It also validates the predictive power of the selected pharmacophore model by performing the ROC and percentage screen analyses. The discrimination between the active and inactive compounds showed that the pharmacophore model was suitable for successfully recognising the biologically relevant molecules as a first filtering step for further computational procedures.

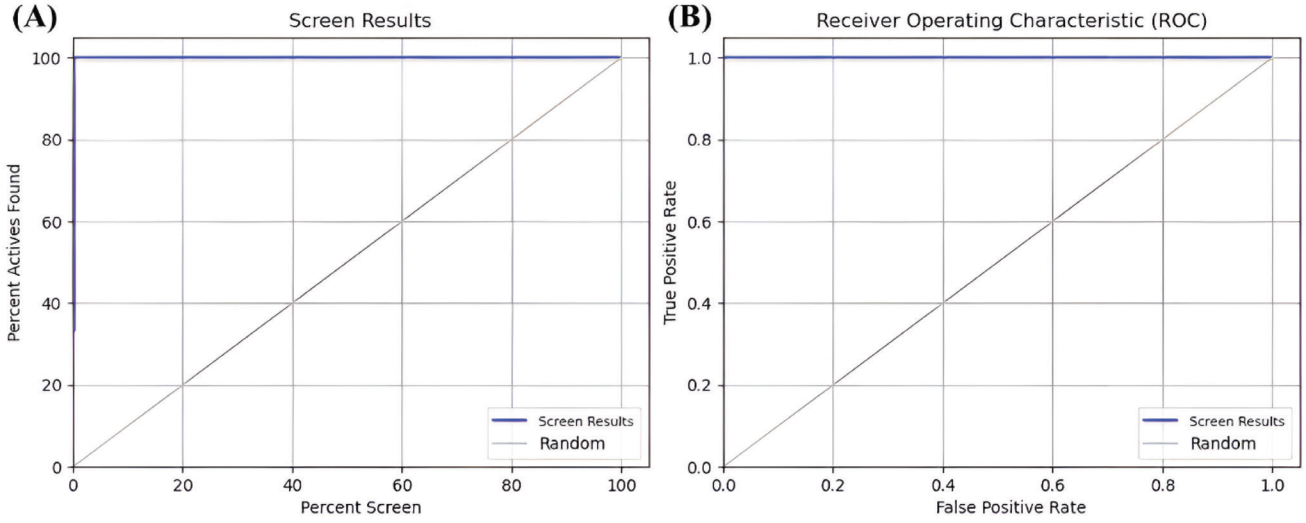

Figure 8: Validation of Pharmacophore Model (A) Percent Plot; (B) ROC Plot

3.3. Analysis of 3D-QSAR Validation

The 3D-QSAR analysis provided extensive data sets for creating predictive models and testing them. The experimental and predicted activities from the training set and test set showed a close agreement, which was a confirmation of the predictive reliability of the developed 3D-QSAR models. The good correlation supports the use of such models for predicting the biological activity of new compounds designed during R-group optimization, as shown in Figure 9. The gradual improvement of the model performance (with several PLS factors) confirmed the statistical robustness of the optimized atom-based QSAR model. The statistical results justify its use for interpretation of structure-activity relationships and prediction of the inhibitory activities of newly designed analogs (Table 6). Table 7 shows that the electron-withdrawing effects and hydrophobic interactions were the most important features contributing to α-glucosidase inhibitory activity, followed by hydrogen bond donor properties. The results straight-away informed the choice of hydrophobic and electron-withdrawing substituents for the generation of the R-group library. Several statistical parameters such as coefficient of determination (R^2), cross-validated coefficient (Q^2), standard deviation (SD), F-test, p-value, root mean square deviation (RMSD), and Pearson correlation coefficient (Pearson-r) were used to evaluate the developed models. High R^2, Q^2, F-test, and Pearson-r values and low SD, RMSD, and p-values represent a reliable and predictive 3D-QSAR model with excellent model accuracy and predictive ability. Table 9 shows that steric and hydrophobic fields contribute most strongly to inhibitory activity, indicating that appropriate molecular size and hydrophobic complementarity are the principal determinants governing α-glucosidase inhibition. These observations further supported the selection of bulky hydrophobic substituents during lead optimization. The first three models generated were found to have relatively low Q^2, R^2, and R^2 scramble and were therefore not found to be the best prediction models. The optimized model, on the other hand, exhibited better statistical performance. In the atom-based 3D-QSAR model, the molecular descriptors include atoms that are hydrogen bond donors (HBD), hydrophobic/non-polar, positively ionizable, and electron-withdrawing (Figure 8). The atom-type fraction map was used to visualize their contributions to biological activity. Moreover, there was a good correlation between the activities of the training set compounds and their respective

predicted values as shown in the scatter plot in Figure 11, where the scatter is centered around the regression line, passing through the origin, giving additional support for the robustness and predictive reliability of the generated QSAR model.

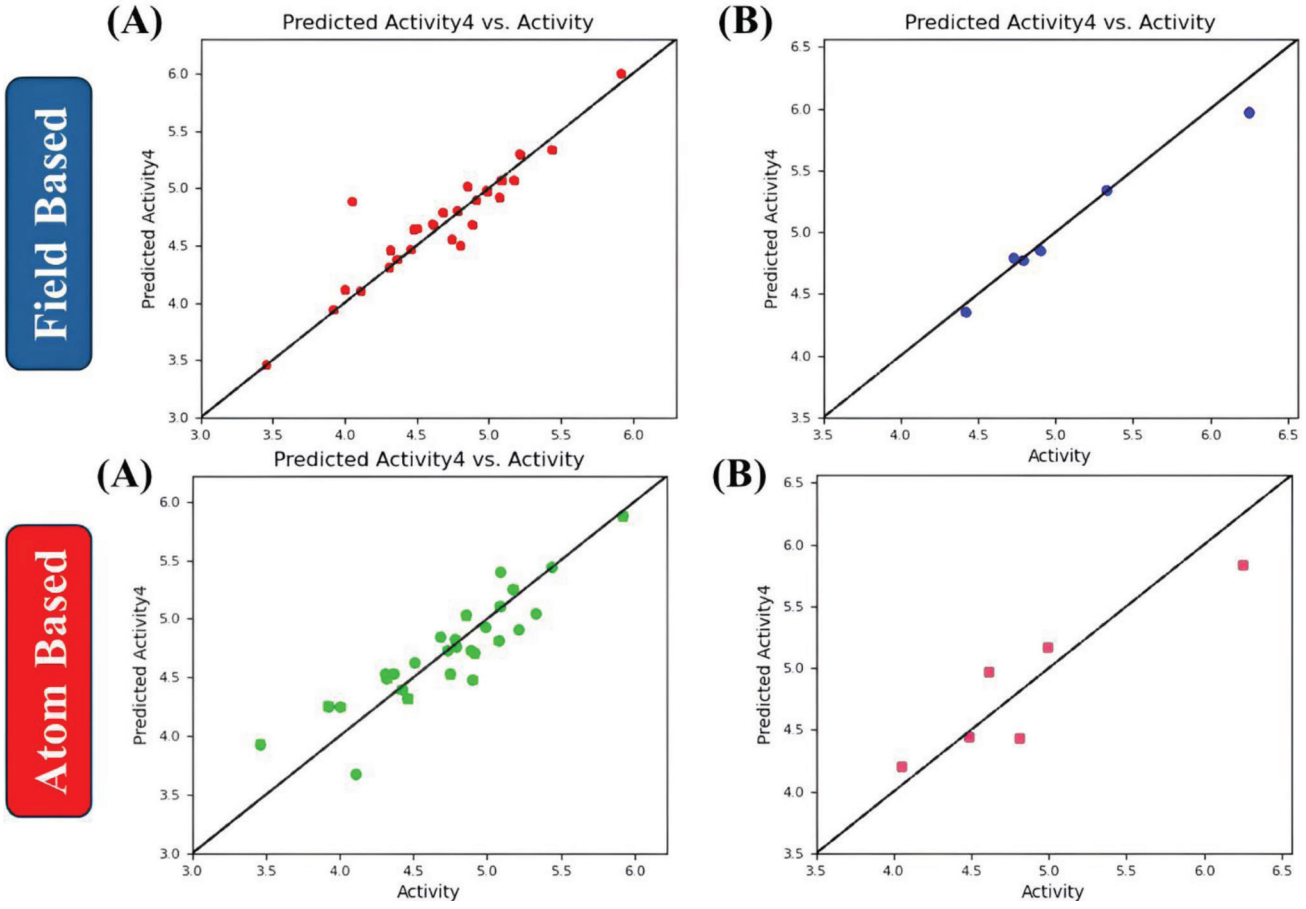

Figure 9: Relationship between the (A) Training and (B) Test Set Data's Actual and Predicted IC_{50} values (Atom & Field based)

3.4. Evaluation of Contour Map

3.4.1. Atom-based 3D-QSAR Models

An atom-based 3D-QSAR model was created to study the role of hydrogen bond donor (HBD), hydrophobic/non-polar, and electron-withdrawing molecular properties on α-glucosidase inhibitory activity. This model gives detailed information on contributions from different atoms and was a good predictor for the biological activity of structurally related compounds. Table 7 summarizes the statistical performance of the model developed using 3D-QSAR-based atoms. The molecular field contour maps were created to show the good and bad spatial areas that control α-glucosidase inhibitory activity. These contour maps were then analyzed, and it was found that the hydrophobic/non-polar field had the highest contribution towards the observed inhibitory activity, showing the importance of hydrophobic interactions in the binding of a ligand. The second most important descriptor was the electron-withdrawing field, suggesting that electron-withdrawing substituents have a favorable effect on enzyme inhibition. The hydrogen bond donor (HBD) field had the lesser contribution, indicating that the studied compounds had a relatively small contribution to their inhibitory potency (Figure 10). The results showed that the hydrophobic interactions have a more significant contribution to increasing the biological activity of α-glucosidase inhibitors when compared to hydrogen bond donor features in the 1,3,4-thiadiazole derivatives.

3.4.1.1. Hydrogen Bond Donor Features

The atom-based 3D-QSAR model-derived contour maps were shown, which describe regions that contain groups of atoms that were important for α-glucosidase inhibitory

activity and act as hydrogen bond donors (HBD). The contour map shows light blue cubes (positive) representing good binding positions, where hydrogen bond donor groups, such as -NH, -NH_2, or -OH, were placed, which could increase the binding affinity of the ligand by forming strong hydrogen bonds with specific amino acid residues in the active site of α-glucosidase. Hence, these replacements are likely to enhance binding affinity and enhance inhibitory activity. Light orange cubes are the unfavorable (negative) regions in the hydrogen bond donor (HBD) contour map, where the introduction of hydrogen bond donor groups was expected to reduce α-glucosidase inhibitory activity. This is a negative effect that can result from steric hindrance or spatial limitations in the enzyme binding pocket that hinder ligand binding to the enzyme and thus reduce biological activity (Figure 10A).

3.4.1.2. Hydrophobic/Non-Polar Features

The hydrophobic (non-polar) contour map obtained from the atom-based 3D-QSAR model represents the contribution of hydrophobic substituents to the α-glucosidase inhibitory activity of the designed 1,3,4-thiadiazole derivatives. The favorable (green) regions on the contour map suggest that hydrophobic substituents (methyl, ethyl, propyl, isopropyl, tert-butyl, cycloalkyl, or aromatic rings) incorporated at these positions should increase inhibitory activity. These groupings help the stabilization of the binding affinity of the ligand to the non-polar part of the active site of α-glucosidase through hydrophobic and van der Waals interactions. On the other hand, purple cubes denote unfavorable (negative) regions, indicating that bulky hydrophobic substituents introduced in the unfavorable regions may affect the optimal orientation of the ligand in the binding pocket, decrease the favorable protein-ligand interactions, and, therefore, decrease the inhibitory activity of α-glucosidase (Figure 10B).

3.4.1.3. Electron-withdrawing Features

The electron-withdrawing (EWG) contour map derived from the 3D-QSAR model shows the spatial effect of electron-withdrawing substituents on the α-glucosidase inhibitory activity of the designed 1,3,4-thiadiazole derivatives. The contour map shows the red cubes as favorable (positive) regions, which means that the placement of electron-withdrawing groups (e.g., -F, -Cl, -CF_3, -CN, -NO_2, carbonyl groups) at these points may improve inhibitory activity. Such substitution enhances the electron distribution of the molecule and helps to increase the binding affinity toward the protein and to stabilize the protein-ligand complex because of an improved interaction with the complementary amino acid residues inside the α-glucosidase active site. On the other hand, blue cubes signify unfavorable (negative) regions, and the introduction of electron-withdrawing groups in these areas could affect the optimal electronic environment, thereby impair protein-ligand recognition and ultimately result in lowered α-glucosidase inhibitory activity (Figure 10C).

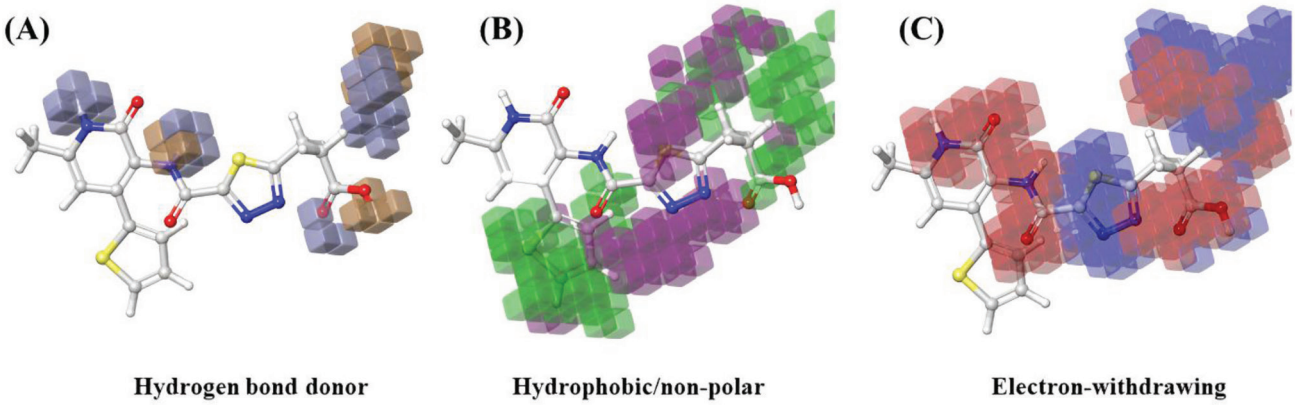

Figure 10: Atom-based 3D-QSAR Models Colouring Representation of (A) Hydrogen Bond Donor; (B) Hydrophobic/Non-Polar; (C) Electron Withdrawing

Table 6: Data Set Analysis of Atom-based QSAR Model

Factors	SD	R^2	R^2 CV	R^2 Scramble	Stability	F	P	RMSE	Q^2	Pearson-r
1	0.4763	0.5728	0.6757	0.5333	0.886	85.4	0.0278	0.61	0.1959	0.5043
2	0.371	0.5174	0.5824	0.6407	0.579	113.4	0.000111	0.24	0.8725	0.9379

3	0.3247	0.6453	0.7262	0.6957	0.773	114.6	1.31e-05	0.2	0.9162	0.9635
4	0.2493	0.7995	0.7348	0.7976	0.811	122.9	9.61e-08	0.29	0.8223	0.9131

Table 7: Atom-type Fraction 3D-QSAR Statistics

Factors	H-bond donor	Hydrophobic/ non-polar	Electron-withdrawing
1	0.037	0.615	0.256
2	0.039	0.671	0.236
3	0.04	0.687	0.22
4	0.043	0.718	0.186

3.4.2. Gaussian Field-based 3D-QSAR Models

The 3D-QSAR model was based on the Gaussian field method to understand the role of steric, electrostatic, hydrophobic, hydrogen bond acceptor (HBA), and hydrogen bond donor (HBD) molecular fields in the α-glucosidase inhibitory activity. Independent molecular alignment was carried out to determine the structural features that led to improved enzyme inhibition. The statistical parameters of the Gaussian field-based 3D-QSAR model possess excellent statistical quality and predictive performance. Together with the atom-based model, it provides complementary evidence supporting the reliability of the identified structure–activity relationships (Table 8). Based on the generated molecular fields, contour maps were drawn that visualize the favorable and unfavorable regions responsible for the biological activity of the designed compounds. The field contributions of the steric field had the most significant effect on α-glucosidase inhibition, followed by the hydrophobic, hydrogen bond acceptor (HBA), and electrostatic fields. The hydrogen bond donor (HBD) field exhibited the least contribution to the measured inhibitory activity (Figure 11).

3.4.2.1. Steric Features

The steric contour plot obtained from the Gaussian field-based 3D-QSAR model showed the size and steric effect of the designed 1,3,4-thiadiazole derivatives on the α-glucosidase inhibitory activity. The contour map showed the green areas as favorable (positive) positions where the addition of moderately bulky groups, like alkyl, cycloalkyl, or aromatic groups, was likely to improve inhibitory activity. These substituents enhance the steric complementarity in the α-glucosidase binding pocket and contribute to the formation of more stable and potent interactions with the receptor through hydrophobic interactions. Yellow contours represent unfavorable (negative) steric regions, indicating that the introduction of bulky substituents at these positions was likely to cause steric clashes with the active site, thereby disrupting optimal ligand orientation and reducing binding affinity, ultimately leading to decreased α-glucosidase inhibitory activity (Figure 11A).

3.4.2.2. Hydrophobic Features

The hydrophobic contour map obtained from the Gaussian field-based 3D-QSAR model showed the hydrophobic contribution from the different substituents in the 1,3,4-thiadiazole family to the α-glucosidase inhibitory activity of the designed molecules. Violet contours were considered favorable (positive) areas that would merit the introduction of hydrophobic substituents, including methyl, ethyl, isopropyl, tert-butyl, cycloalkyl, and/or aromatic rings at these positions for enhancing their inhibitory activity. These groups enhance the affinity of the ligand to the non-polar parts of the α-glucosidase active site and enhance the stability of the protein-ligand complex. On the other hand, unfavorable (negative) regions, displayed in sky-blue color, indicated that the introduction of hydrophobic groups in such regions may cause loss of the optimal orientation of the ligand, decrease the interactions between the relatively polar parts of the binding pocket and the hydrophobic groups, and decrease the binding efficiency, which may result in a decreased α-glucosidase inhibitory activity (Figure 11B).

3.4.2.3. Hydrogen Bond Donor Features

Contour maps derived from the hydrogen-bonded field-based 3D-QSAR model showed that the hydrogen bond donor functionalities contributed to the α-glucosidase inhibitory activity of the designed 1,3,4-thiadiazole derivatives. The pink contours on the contour map represent favorable (positive) regions; hydrogen bond donor groups (such as -NH, -NH_2, -OH, or amide NH) at these positions could be useful for increasing inhibitory activity. The interactions increase the affinity for the binding of the ligand and help in the stabilization of the protein-ligand complex. Unfavorable (negative) shaded regions were in light violet, which means that the introduction of hydrogen bond donor groups in these areas could cause the ligand to lose its optimal orientation, steric or electronic restrictions, or favorable interactions within the binding pocket, leading to decreased α-glucosidase inhibitory activity (Figure 11C).

3.4.2.4. Hydrogen Bond Acceptor Features

The 3D-QSAR model constructed by Gaussian field was used to generate the hydrogen bond acceptor (HBA)

contour map showing the spatial contribution of hydrogen bond acceptor functionalities to the inhibitory activity of the designed 1,3,4-thiadiazole derivatives against α-glucosidase. The contour map shows that the black contour regions represent favorable (positive) positions, in which it is likely to increase inhibitory activity if hydrogen bond acceptor groups like carbonyl (C=O), ether oxygen (-O-), ester oxygen, sulfoxide, or nitrogen-containing heterocyclic moieties are introduced. Such functional groups can engage in intense hydrogen bonding with complementary amino acid residues in the α-glucosidase active site, enhance the binding affinity of the ligand, and stabilize the protein-ligand complex. Regions showing unfavorable (negative) contours were indicated as light green-colored regions, and such groups that may be introduced at these positions could either interfere with the optimal interaction pattern or provide an unfavorable electronic environment or change the correct orientation of the ligand in the binding pocket, thus resulting in a decreased α-glucosidase inhibitory activity (Figure 11D).

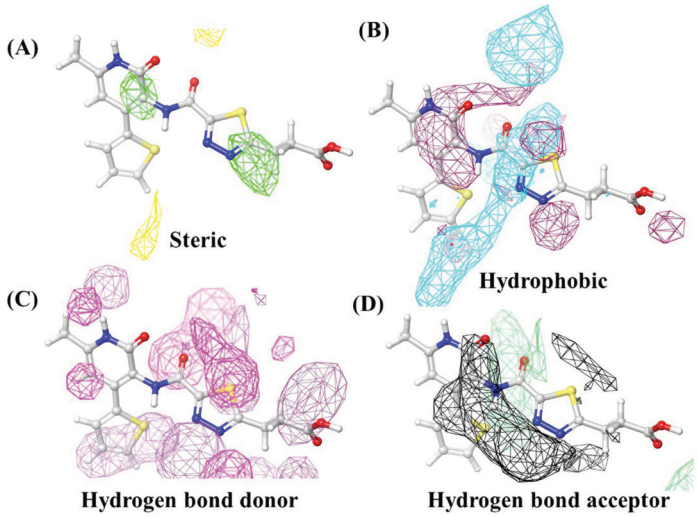

Figure 11: Gaussian Field-based 3D-QSAR Models Colouring Representation of (A) Steric; (B) Hydrophobic; (C) Hydrogen Bond Donor; (D) Hydrogen Bond Acceptor

Table 8: Data Set Analysis of Gaussian Field-based QSAR Model

Factors	SD	R^2	R^2 CV	R^2 Scramble	Stability	F	P	RMSE	Q^2	Pearson-r
1	0.3757	0.4853	0.5717	0.4883	0.647	84.5	3.82e-05	0.57	0.5177	0.6144
2	0.2072	0.8494	0.7591	0.7458	0.698	105.5	5.26e-11	0.43	0.6091	0.8147
3	0.1309	0.9423	0.7638	0.8442	0.713	130.7	5.31e-15	0.4	0.6661	0.8256
4	0.1018	0.9666	0.8281	0.8856	0.827	166.2	1.29e-16	0.39	0.6816	0.8446

Table 9: Gaussian Field-based Fraction 3D-QSAR Statistics

Factors	Gaussian Steric	Gaussian Electrostatic	Gaussian Hydrophobic	Gaussian H-bond Acceptor	Gaussian H-bond Donor
1	0.471	0.107	0.207	0.127	0.088
2	0.412	0.116	0.235	0.136	0.101
3	0.409	0.116	0.235	0.125	0.115
4	0.406	0.117	0.238	0.12	0.119

3.5. Molecular Docking Analysis

A set of 5 compounds (25, 27, 30, 33, and 34) were selected from the earlier data set and subjected to molecular docking analysis with the α-glucosidase catalytic pocket, which showed favorable binding with an interaction profile similar to that of the reference inhibitor Acarbose (Figure 12). Before docking analysis of the dataset compounds, the docking protocol was validated by re-docking the co-crystallized ligand (acarbose) into the active site of α-glucosidase. The re-docked ligand was found to be in the same binding orientation as the experimental structure with an RMSD that was less than the generally accepted limit of 2.0 Å. Furthermore, the proper key hydrogen-bond interactions with catalytic residues such as Asp282, Asp404, Asp518, Asp616, Arg600, and His674 were captured, which indicated that the docking protocol correctly predicts the binding conformation of the ligand in the α-glucosidase active site. Of the compounds in the dataset, compound 25 had the highest docking score of -6.686 kcal/mol. It forms hydrogen bond interactions with Arg281, Asp282, Asp518, Asp616, and Arg600, along with π-π stacking with Phe649 and a large extent of hydrophobic interactions with Leu283, Ala284, Met519, Trp516, Trp376, Trp481, Leu405, Leu650, Leu677, Leu678, Ile441, Phe525, and His674, forming a stable binding conformation in the active site. Compound 27 also had a docking score of -6.549 kcal/mol, forming hydrogen bonds with Asp616, Asp518, Arg600, and Asn524, and having additional hydrophobic interactions with Leu283, Ala284, Met519, Trp516, Leu405, Trp481, Leu650, Leu677, Leu678, Phe525, Ser523, and His674. The docking score obtained by Compound 33 is -6.356 kcal/mol, and it forms various docking interactions, including π-π stacking with Phe649 and hydrophobic interactions with Met519, Trp516, Trp376, Trp481, Leu405, Leu677, Ser676, His674, and hydrogen bonding with Asp282, Arg281, and Asp518. Likewise, compound 34 gave a docking score of -6.122 kcal/mol and forms hydrogen bonding with Arg281, Asp282, Arg600, and Asp518, in addition to π-π stacking with Phe649 and hydrophobic interactions with Leu283, Ala284, Met519, Trp516, Trp481, Leu405, Leu650, Leu677, Leu678, Phe525, and His674. The docking score of compound 30 was -5.959 kcal/mol, which maintained a stable binding orientation by hydrogen bond with Trp618, Arg600, Asp518, and Asp616; π-π stacking with Trp376; and hydrophobic interactions with Leu283, Ala284, Met519, Trp516, Leu405, Leu650, Leu677, Leu678, Ile441, Phe649, and His674. The selected dataset of compounds shared several conserved interactions with Arg281, Asp282, Arg600, Asp518, Asp616, Met519, Phe649, Trp516, Leu405, and His674, which play an important role in the recognition and stabilization of a ligand inside the α-glucosidase active site. Acarbose, a reference inhibitor, had the highest binding affinity (-11.894 kcal/mol), with the formation of an extensive hydrogen-bonding network with Arg281, Asp282, Asp404, Asp518, Asp616, Arg600, His674, Gly615, and Arg672, in addition to several hydrogen-mediated interactions due to its highly hydroxylated structure.

The R-group designed derivatives (DM01, DM02, and DM03) were then docked into the same α-glucosidase binding pocket to assess the effect of structural optimization. In general, the above results suggested that the structure-guided R-group modifications were able to increase the interactions of the ligands with the protein without compromising the important pharmacophoric features identified in the previous computational studies (Figure 13). The designed compounds showed higher binding affinity than all other compounds with a docking score of -8.592 kcal/mol with hydrogen bonds with Asp518, Arg600, Asp282, and Trp376; π-π stacking with Phe649; and hydrophobic interactions with Met519, Trp516, Leu405, Trp481, Ile441, Leu650, Leu677, Ser676, His674, Phe525, and Ala555. DM02 formed the following hydrogen-bond interactions with Arg600, Asp518, Trp618, and Asp616, as well as with Phe649 and Trp481 through π-π stacking and hydrophobic interactions with Leu283, Ala284, Pro285, Pro287, Met519, Trp516, Trp376, Trp613, Leu650, Leu677, Leu678, Ser676, His674, and Gln623. Similarly, the docking score for DM03 was calculated as -8.439 kcal/mol and was found to interact with Arg600, Asp518, Asp404, and the ligand carbonyl oxygen, along with π-π stacking with Phe649 and hydrophobic interactions with Leu283, Ala284, Met519, Trp516, Trp481, Trp613, Leu650, Leu677, Ser676, and His674. All the designed derivatives interacted with the conserved catalytic residues Arg600, Asp518, Met519, Trp516, Phe649, Leu405, His674, and Trp481, suggesting their important role in the stabilization of ligand binding to the α-glucosidase active site. Furthermore, the improved docking scores for DM01, DM02, and DM03 compared with the parent set compounds indicate that the derivatives designed in this study were more likely to interact with the binding site than the parent set, thus enhancing the binding affinity of the 1,3,4-thiadiazole scaffold, although these are less potent than the reference inhibitor acarbose.

3.6. Virtual Screening Results of R-Group-Enumerated Compounds

Using a strategy of electron withdrawal and diversity of hydrophobic groups, a virtual library of 1,419 novel 1,3,4-thiadiazole derivatives was created. The library was then screened using a hierarchical virtual screening

strategy in Schrödinger Maestro version 12.5. All compounds were first screened by the High-Throughput Virtual Screening (HTVS) protocol. The molecules in the top 50% of the HTVS-ranked molecules were then re-docked with the Standard Precision (SP) protocol, and the top 20% of the SP hits were further re-docked using the Extra Precision (XP) protocol. Finally, optimized lead candidates were selected for detailed analysis from the top 10% of XP-docked compounds. Among these identified 14 compounds, three compounds, DM01, DM02, and DM03, were found to have the best docking scores of -8.592, -8.486, and -8.439 kcal/mol, respectively, with XP docking scores represented in Table 10. Detailed docking analysis revealed that DM01 had the highest binding affinity to the receptor, as it established hydrogen-bond and π-π stacking interactions with Asp518, Arg600, Asp282, Trp376, and Phe649, respectively, in addition to hydrophobic interactions with Met519, Trp516, Leu405, Trp481, Ile441, Leu650, Leu677, Ser676, His674, Phe525, and Ala555. DM02 exhibited a docking score of -8.486 kcal/mol and established hydrogen bonds with Arg600, Asp518, Trp618, and Asp616, while Phe649 and Trp481 participated in π-π stacking and hydrophobic interactions with Leu283, Ala284, Pro285, Pro287, Met519, Trp516, Trp376, Trp613, Leu650, Leu677, Leu678, Ser676, His674, and Gln623. Likewise, DM03 had a docking score of -8.439 kcal/mol and displayed hydrogen bond interactions with Arg600, Asp518, Asp404, and the ligand carbonyl oxygen, π-π stacking with Phe649, and hydrophobic interaction with Leu283, Ala284, Met519, Trp516, Trp481, Trp613, Leu650, Leu677, Ser676, and His674. Overall, the designed derivatives consistently interacted with the conserved catalytic residues Arg600, Asp518, Met519, Trp516, Phe649, Leu405, His674, and Trp481, as these amino acid residues were important for the recognition and stabilization of the ligand within the active site of α-glucosidase. The better docking scores and preserved interaction profiles of DM01, DM02, and DM03 compared with the parent dataset compounds suggest that R-group optimization has effectively improved the binding affinity of the 1,3,4-thiadiazole scaffold, making these derivatives good candidates to develop as α-glucosidase inhibitors.

3.7. Prediction of ADME Properties

The drug-likeness and pharmacokinetic properties of selected dataset compounds (25, 27, 30, 33, and 34) were compared with the drug-activity counterpart acarbose, using the ADME profiles. Acarbose had the highest molecular weight (645.611 g/mol) and the largest solvent-accessible surface area (855.709 Å²), along with a high hydrogen-bonding capacity (14 hydrogen bond donors and 32.1 hydrogen bond acceptors). It was highly hydrophilic with extremely low lipophilicity (QPlogPo/w = -7.423) and very low permeability (Caco-2 = 0.036 nm/s; MDCK = 0.008 nm/s) and very low 0% predicted human oral absorption, which is consistent with the highly hydrophilic properties and local action in the intestine. The molecular weights of the selected compounds, however, were significantly lower (382.393-438.475 g/mol), while the solvent-accessible surface area was within the moderate range (647.258-744.479 Å²), suggesting better physicochemical properties for oral drug development. The number of hydrogen bond donors varied from 2.25 to 3.25, and the number of hydrogen bond acceptors was 8.25 to 11.65. All compounds had an appropriate balance between aqueous solubility and membrane permeability, with log Po/w from 1.857 to 3.279. Compound 34 was the most lipophilic compound (3.279), while compound 30 was the least lipophilic (1.857). The Caco-2 permeability for the compounds ranged from 6.721 nm/s (compound 30) to 17.828 nm/s (compound 33), and the MDCK permeability for the compounds ranged from 3.852 nm/s (compound 30) to 18.918 nm/s (compound 34), showing better permeability in the membrane. The QPlogBB values for all the dataset compounds were good (-2.628 to -2.041), indicating that the compounds have limited BBB penetration, which was desired for a potential α-glucosidase inhibitor designed for an extra-central nervous system effect. Similarly, the values of QPlogKhsa (-0.305 to 0.132) were also within the acceptable range for plasma protein binding. Human oral absorption values were predicted to be between 52.63% and 68.41%, with compound 34 having the highest, compound 33 the second highest, and compound 30 the lowest value. In addition, none of the compounds in the dataset were in violation of the Lipinski Rule of Five, whereas one or two Rule of Three violations were found, indicating that they are generally drug-like. The selected dataset compounds showed significantly higher lipophilicity, membrane permeability, and oral absorption when compared to acarbose, which would make them good candidates as orally active α-glucosidase inhibitors. Finally, it was important to note that the models developed in the present study can only be used to a certain extent in the chemical space of the investigated 1,3,4-thiadiazole derivatives. Extensive statistical validation of the dataset resulted in a good degree of robustness and predictive power of the model, even though only 34 compounds were included. However, their generalizability and predictive capabilities could be further enhanced with more structurally diverse analogues and model validation with more external compounds.

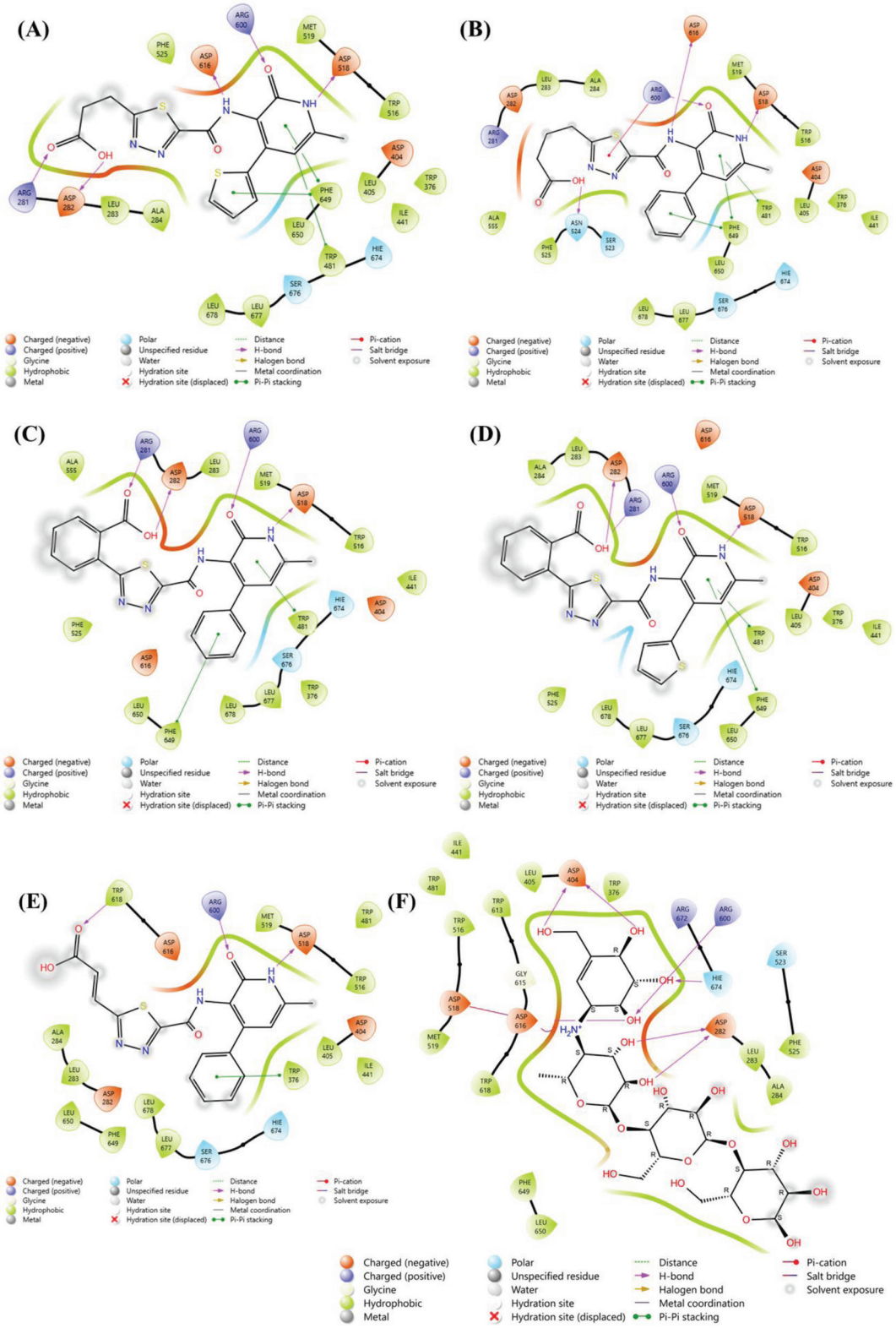

Figure 12: 2D Interactions of Data Set Compounds with α-Glucosidase (PDB ID: 5NN8)- (A) Compound 25, (B) Compound 27, (C) Compound 33, (D) Compound 34, (E) Compound 30, (F) Acarbose (Reference)

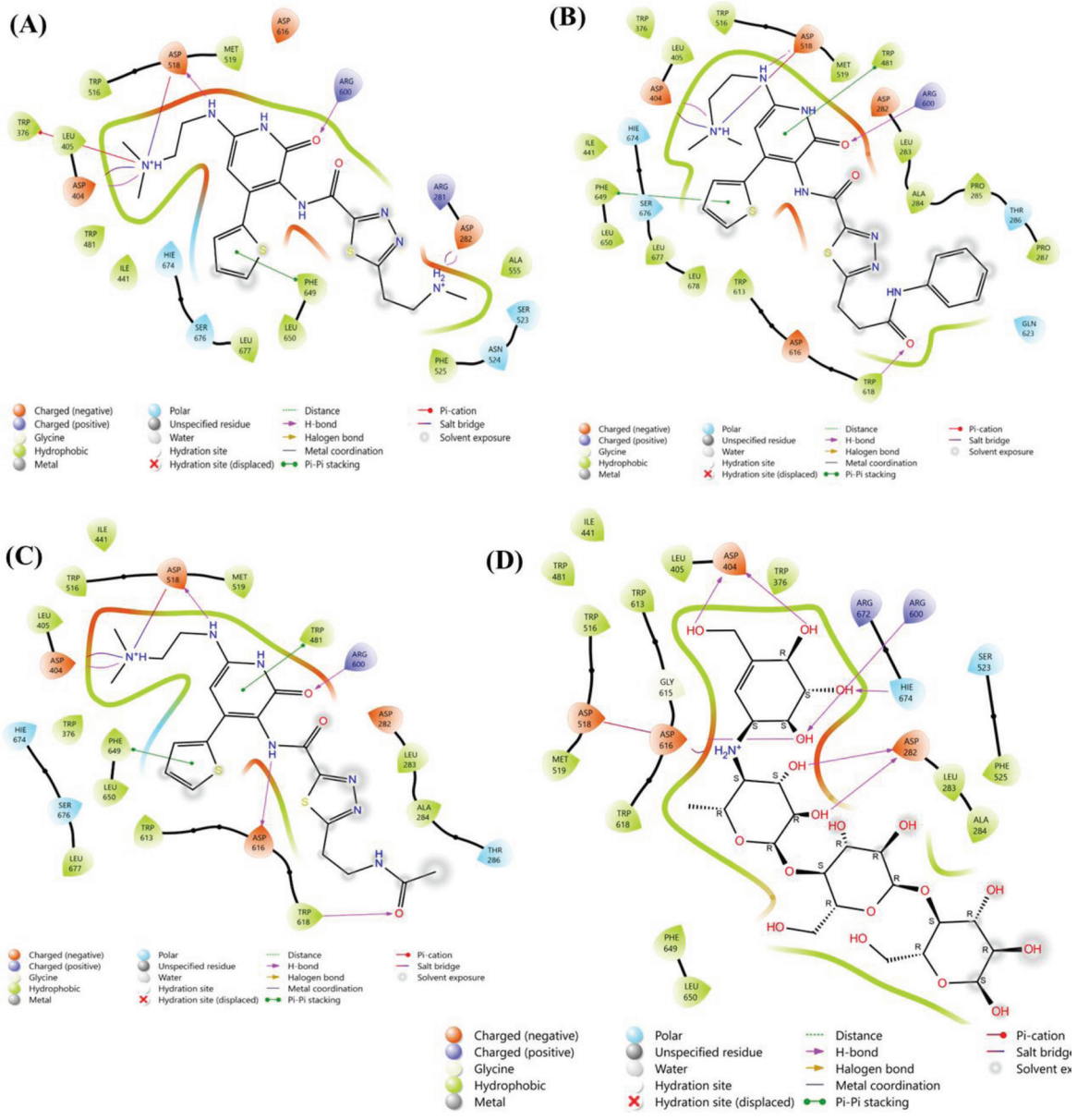

Figure 13: 2D Interactions of R-group Compounds (designed) with α-Glucosidase (PDB ID: 5NN8)- (A) Compound DM01, (B) Compound DM02, (C) Compound DM03, (D) Acarbose (Reference)

Table 10: Docking Scores (DS) of Dataset Compounds, R-group Enumerated Compounds**,** and Acarbose (reference compound)

Name of Compounds	**Structure**	**DS (xp) kcal\mol**	**Interaction with Amino Acid Residues**
25	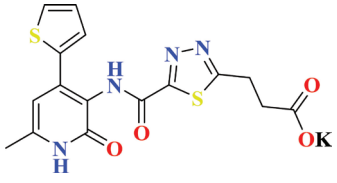	-6.686	ARG600, ASP616, ASP518, PHE649, LEU650, TRP481, ARG281, ASP282

27	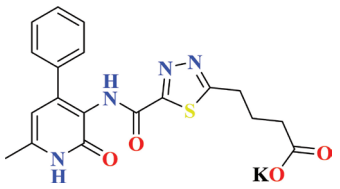	-6.549	ASN524, ARG600, ASP616, ASP518, TRP481, PHE649
33	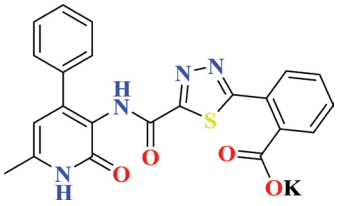	-6.356	ARG281, ASP282, ARG600, ASP518, TRP481, PHE649
34	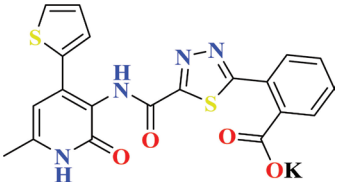	-6.122	ASP282, ARG600, TRP481, PHE649, ASP518
30	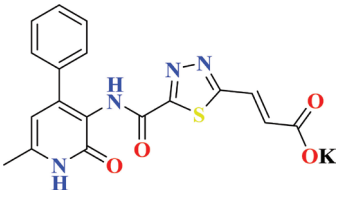	-5.959	TRP618, ARG600, ASP518, TRP376
DM01	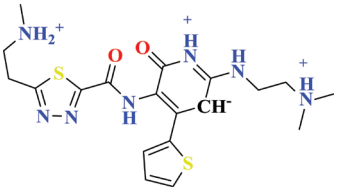	-8.592	TRP376, LEU405, ASP518, ARG600, PHE649, ASP282
DM02	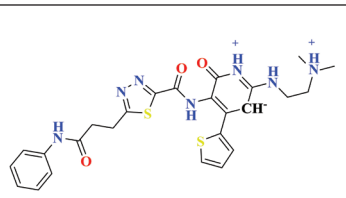	-8.486	ASP518, TRP481, ARG600, ASP404, PHE649, TRP618
DM03	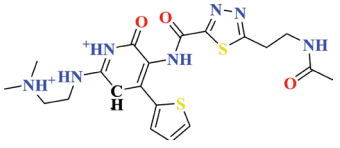	-8.439	ASP404, ASP518, TRP481, ARG600, TRP618, ASP616, PHE649
Acarbose	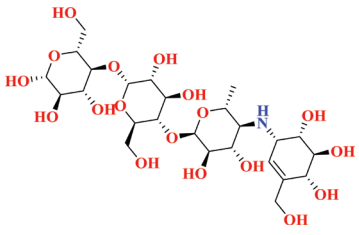	-11.894	ASP518, ASP616, ASP404, ARG600, HIE674, ASP282

The designed derivatives (DM01, DM02, and DM03) were also evaluated and compared to acarbose for their ADME properties. All three designed molecules exhibited favorable membrane permeability and oral absorption compared with the reference inhibitor, which exhibited low permeability and no absorption. The molecular weights of DM01 (447.572 g/mol), DM02 (491.579 g/mol), and DM03 (537.653 g/mol) were within and near the acceptable range for orally active compounds, and the solvent-accessible areas (759.679-877.933 Å²) represented moderate molecular size. DM01 and DM03 had 3.25 hydrogen bond donors, while DM02 had 2.25 hydrogen bond donors, with all three analogs having relatively high numbers of hydrogen bond acceptors (10.25-11.65) that would facilitate favorable interactions with the target enzyme. The designed compounds showed moderate lipophilicity (QPlogPo/w = 1.505-2.794), which was much higher than acarbose and was favorable for membrane diffusion. Furthermore, all three compounds had good QPlogHERG values (-6.997 to -7.906), suggesting a low predicted risk of cardiotoxicity. The designed analogues showed that DM02 has the highest permeability values in Caco-2 (25.059 nm/s) and excellent permeability values in MDCK (18.725 nm/s), followed by DM03 (21.258 and 15.513 nm/s, respectively) and DM01 (14.203 and 13.921 nm/s, respectively), indicating efficient intestinal absorption and membrane transport. All their QPlogBB values (-1.952 to -0.890) were within acceptable ranges, indicating limited penetration across the blood-brain barrier, and QPlogKhsa values (-0.226 to 0.206) showed plasma protein binding was balanced. The human oral absorption percentage predicted for all 3 compounds ranged between 54.11% (DM03) and 61.96% (DM02), with DM02 having the most favorable human oral absorption percentage. In addition, DM01 and DM02 had no violation of any restriction in Lipinski's Rule of Five, while DM03 had one violation, suggesting that all three designed derivatives have desirable drug-like properties despite the relatively larger molecular sizes (Table 11). The ADMET results demonstrate that the optimized derivatives possess acceptable drug-likeness and pharmacokinetic properties while maintaining favorable physicochemical characteristics for oral administration. When interpreted together with the pharmacophore, QSAR, docking, and virtual screening results, these findings support the prioritization of DM01-DM03 as computationally promising α-glucosidase inhibitor leads suitable for future experimental validation. The overall designed analogues exhibited better pharmacokinetic properties than acarbose and were potential orally active 1,3,4-thiadiazole-based α-glucosidase inhibitors for further investigation**.**

Table 11: ADME Properties of Dataset Compounds, R-group Enumerated Compounds, and Reference Compound Sitagliptin

molecule	mol_ MW	SASA	donor_ HB	accpt_ HB	QPlog_ Po/w	QPlog_ HERG	QPP_ Caco	QPlog_ BB	QPP_ MDCK	QPlog_ Khsa	Percent Human Oral Absorption	Rule Of Five	Rule Of Three
Acarbose	645.611	855.709	14	32.1	-7.423	-5.597	0.036	-5.718	0.008	-2.536	0	3	2
25	390.431	647.258	2.25	8.25	1.927	-3.683	11.736	-2.155	9.265	-0.305	57.372	0	1
27	398.436	700.113	2.25	8.25	2.341	-4.165	8.18	-2.628	4.733	-0.172	56.992	0	1
33	432.453	724.941	2.25	8.25	3.161	-4.986	17.828	-2.061	12.107	0.099	67.847	0	2
34	438.475	744.79	2.25	8.25	3.279	-5.216	17.53	-2.046	18.918	0.132	68.407	0	2
30	382.393	656.955	2.25	8.25	1.857	-4.046	6.721	-2.552	3.852	-0.305	52.63	0	1
DM01	447.572	759.679	3.25	10.25	1.505	-7.142	14.203	-0.89	13.921	-0.078	56.383	0	1
DM02	491.579	811.864	2.25	11.65	1.704	-6.997	25.059	-1.952	18.725	-0.226	61.961	0	1
DM03	537.653	877.933	3.25	11.25	2.794	-7.906	21.258	-2.099	15.513	0.206	54.109	1	1

Representation of: (QPlog Po/w) Octanol/water partition coefficient; (QPPCaco) cell permeability (nm/s); (QPlogBB) Brain/blood partition coefficient (QPPMDCK) Apparent MDCK cell permeability (nm/s) (SASA) Solvent-accessible surface area; Human serum albumin binding: 6% human oral absorption.

4. Optimisation of Novel Ligands

The derivatives designed (DM01-DM03) have to be considered lead candidates for computation but not as tested inhibitors. They were selected based on a pharmacophore model, validated 3D-QSAR models, molecular docking, SAR analysis and prediction of ADMET. These integrated computational approaches provide higher confidence in prioritising the leads, but the proposed compounds were still hypothetical until they were synthesised, characterised, evaluated for activity in enzymes, and profiled for biological activity. Further studies will thus be directed towards the synthesis of these derivatives, *in vitro* α-glucosidase inhibition tests and further pharmacological studies to confirm the computational predictions. The integrated

interpretation of the AADHR_3 pharmacophore model in conjunction with the atom-based and Gaussian field-based 3D-QSAR contour maps established the structure-activity relationship (SAR) of the 1,3,4-thiadiazole scaffold. The SAR study showed that bulky hydrophobic groups such as phenyl, substituted phenyl, cycloalkyl, alkyl, benzyl and heteroaromatic groups at the R_1 position resulted in an increase of the α-glucosidase inhibitory activity by increasing favourable hydrophobic and steric interactions with the enzyme binding pocket. However, substituents with bulky, polar, charged, or hydrogen-bond donors at the R_1 position were observed to decrease inhibitory activity due to steric hindrance and unfavourable orientation of the ligand. Likewise, the substitution of electron-withdrawing groups at the R_2 position (-F, -Cl, $-CF_3$, -CN, $-NO_2$, -COOR, $-CONH_2$ and $-SO_2R$) was predicted to improve inhibitory activity by means of more favourable electronic interactions with the active site of the α-glucosidase inhibitory activity. On the contrary, the introduction of $-OCH_3$, $-CH_3$, and $-NH_2$ and overcrowding of the R_2 position were found to decrease inhibitory potency (Figure 14). The combination of the results obtained from the pharmacophore and 3D-QSAR analyses suggests that the structural modification at the R_1 position with the introduction of hydrophobic substituents at the R_2 position with electron-withdrawing substituents would be the most appropriate direction for the rational design of potent α-glucosidase inhibitors.

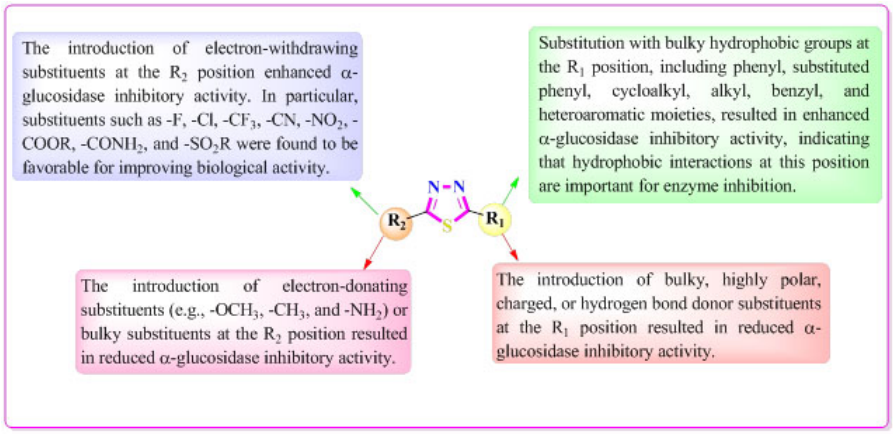

Figure 14: SAR of the 1,3,4-Thiadiazole Moiety as α-Glucosidase Inhibitory Activity

5. Limitations of the Study

Although a wide range of computational workflows was used in this study, there are some restrictions that should be noted. The pharmacophore modelling, 3D-QSAR analyses, molecular docking, virtual screening and ADMET prediction all make important contributions to understanding in terms of the structural determinants of α-glucosidase inhibition and rational prioritisation of lead compounds. These computational methods, however, constitute predictive models and do not totally mimic the complexity of biological systems. Molecular docking also compares rigid protein-ligand complexes with simpler scoring functions and does not fully consider protein flexibility, protein-solvent interactions, conformational changes, and entropic factors. Similarly, the 3D-QSAR models can be used for structures that were only explored in the investigated 1,3,4-thiadiazole derivatives chemical space and could not be used with compounds that are completely different in structure. Moreover, the ADMET values reported here have theoretical values, which should be confirmed by experiments. Most importantly, the designed compounds (DM01, DM02 and DM03) have not been synthesised or tested for their inhibitory activity and binding affinity *in vitro* α-glucosidase enzyme inhibition assays. Therefore, the present results should be taken as a rational computational approach to identify leads and not as proof of biological activity.

6. Conclusion

In conclusion, a computer-aided drug design approach, including the pharmacophore modelling, atom-based and Gaussian field-based 3D-QSAR analyses, R-group enumeration, virtual screening, molecular docking and ADMET prediction, was found effective for the investigation of the structure-activity relationships of 1,3,4-thiadiazole derivatives as possible α-glucosidase inhibitors. A combination of complementary computational analyses led to the identification of key structural features that were used to develop three lead candidates (DM01, DM02, and DM03) with good predicted binding interactions and acceptable PK properties. The results, however, are derived solely from *in*

silico analysis and are, therefore, valid only as computational predictions and not as proof of bio-efficacy. The present models were developed with a relatively small but structurally consistent dataset, but the models were extensively statistically validated and were found to be reliable for prediction in the range of the investigated space of chemical structures. Future studies to assess the compound's potential as novel α-glucosidase inhibitors should include chemical synthesis of the proposed derivatives and *in vitro* α-glucosidase enzyme inhibition studies, enzyme kinetic studies, and additional pharmacological studies of larger and structurally more diverse datasets and computational predictions.

Abbreviations

3D-QSAR: Three-Dimensional Quantitative Structure-Activity Relationship; **DM**: Diabetes Mellitus; **HBA:** Hydrogen Bond Acceptor; **HBD:** Hydrogen Bond Donor; **LOO:** Leave-One-Out; **PLS:** Partial Least Square; **RMSD:** Root Mean Square Deviation; **SASA:** Solvent Accessible Surface Area; **SD:** Standard Deviation; **T2DM:** Type 2 Diabetes Mellitus; **HTVS:** high-throughput virtual screening; **PDB:** Protein Data Bank; **XP:** extra precision; **ADME:** absorption, distribution, metabolism and excretion; **EWGs:** electron-withdrawing groups.

Acknowledgments

The authors sincerely acknowledge the Department of Pharmaceutical Chemistry, SWIFT School of Pharmacy, Rajpura, Punjab, India, and the University School of Pharmaceutical Sciences, Rayat Bahra University, Hoshiarpur, Punjab, India, for providing the academic environment and research facilities necessary for this study. The authors gratefully acknowledge Schrödinger, LLC, New York, NY, USA, for providing access to the Schrödinger Suite under the academic licensing program used in this study. Finally, the authors thank their colleagues and mentors for their valuable discussions and continuous support throughout this research.

Authorship Contribution

Priya Devi conceptualized the present research work and interpreted the molecular docking and 3D-QSAR results. Debarshi Mondal performed the molecular docking study, wrote the original draft and performed 3D-QSAR studies. Shalini Sharma and Harmel Singh Chahal checked the final draft of the manuscript.

Conflict of Interest

The authors declare that there is no conflict of interest regarding this manuscript.

Ethical Approval

The authors declare that no ethical approval was required for this study.

Funding

The authors declare that no specific funding was received from any public, commercial, or not-for-profit funding agency for this research.

Data Availability Statement

This article includes all the data generated or analyzed during this study.

Human and Animal Rights

No animals or human participants were involved in this study.

Figure Permissions

All figures included in this manuscript are original, created by the authors, and don't require permission from any third party. The authors retain the rights to these figures and grant the publisher permission to reproduce them as part of this publication.

AI Disclosure Statement

The authors declare that artificial intelligence (AI) assisted tools were used solely for language enhancement, grammar checking, and improving the readability of the manuscript.

References

Acar Çevik, U., Celik, I., Işık, A., Ahmad, I., Patel, H., Özkay, Y., & Kaplancıklı, Z. A. (2023). Design, synthesis, molecular modeling, DFT, ADME and biological evaluation studies of some new 1, 3, 4-oxadiazole linked benzimidazoles as anticancer agents and aromatase inhibitors. *Journal of Biomolecular Structure and Dynamics, 41*(5), 1944–1958. https://doi.org/10.1080/07391102.2022.2025906

Akdağ, M., Çam, M. G., Ergen, D., Demir, Y., Beydemir, Ş., & Özçelik, A. B. (2025). Synthesis of new Pyridazinone derivatives and their dual inhibitory activity on aldose reductase and α-glucosidase. *Bioorganic & Medicinal Chemistry Letters*, 130498. https://doi.org/10.1016/j.bmcl.2025.130498

Asati, V., Bharti, S. K., & Budhwani, A. K. (2017). 3D-QSAR and virtual screening studies of thiazolidine-2, 4-dione analogs: Validation of experimental inhibitory potencies towards PIM-1 kinase. *Journal of Molecular Structure, 1133*, 278–293. https://doi.org/10.1016/j.molstruc.2016.12.006

Bischoff, H. B. A. G. (1994). Pharmacology of alpha-glucosidase inhibition. *European Journal of Clinical Investigation, 24*, 3–10. https://doi.org/10.1111/j.1365-2362.1994.tb02249.x

Bisht, P., Gautam, P., Bhattacharya, A., Singh, R., & Verma, S. K. (2025). Designing of xanthine-based DPP-4 inhibitors: A structure-guided alignment dependent Multifacet 3D-QSAR modeling, and molecular dynamics simulation study. *Journal of Biomolecular Structure and Dynamics, 43*(13), 6971–6995. https://doi.org/10.1080/07391102.2024.2329787

Chiba, S. (1997). Molecular mechanism in α-glucosidase and glucoamylase. *Bioscience, Biotechnology, and Biochemistry, 61*(8), 1233–1239. https://doi.org/10.1271/bbb.61.1233

Dawood, K. M., & Farghaly, T. A. (2017). Thiadiazole inhibitors: A patent review. *Expert Opinion on Therapeutic Patents, 27*(4), 477–505. https://doi.org/10.1080/13543776.2017.1272575

Gholami Rostami, E., & Fatemi, M. H. (2018). Comparative molecular field analysis and hologram quantitative structure activity relationship studies of pyrimidine series as potent phosphodiesterase 10A inhibitors. *Journal of the Chinese Chemical Society, 65*(11), 1293–1306. https://doi.org/10.1002/jccs.201700435

Gholami Rostami, E., & Fatemi, M. H. (2019). Molecular docking and receptor-based QASR studies on pyrimidine derivatives as potential phosphodiesterase 10A inhibitors. *Structural Chemistry, 30*(6), 2347–2368. https://doi.org/10.1007/s11224-019-01353-6

Gupta, S., Saha, M., Singh, R., Ahmed, S. B., & Asati, V. (2025). Multistage in silico approach to identify novel quinoline derivatives as potential c-kit kinase inhibitors. *Journal of Biomolecular Structure and Dynamics, 43*(11), 5313–5330. https://doi.org/10.1080/07391102.2024.2308759

Hanefeld, M., & Schaper, F. (2007). The role of alpha-glucosidase inhibitors (acarbose). In *Pharmacotherapy of Diabetes: New Developments: Improving Life and Prognosis for Diabetic Patients* (pp. 143–152). Springer US. https://doi.org/10.1007/978-0-387-69737-6_13

Haritha, M., Sreerag, M., & Suresh, C. H. (2024). Quantifying the hydrogen-bond propensity of drugs and its relationship with Lipinski's rule of five. *New Journal of Chemistry, 48*(11), 4896–4908. https://doi.org/10.1039/D3NJ05476D

Hosen, S. Z., Dash, R., Khatun, M., Akter, R., Bhuiyan, M. H. R., Karim, M. R., ... & Afrin, S. (2017). *In silico ADME/T and 3D QSAR analysis of KDR inhibitors. Journal of Applied Pharmaceutical Science, 7*(1), 120–128. https://doi.org/10.7324/JAPS.2017.70116

Hu, Y., Li, C. Y., Wang, X. M., Yang, Y. H., & Zhu, H. L. (2014). 1, 3, 4-Thiadiazole: Synthesis, reactions, and applications in medicinal, agricultural, and materials chemistry. *Chemical Reviews, 114*(10), 5572–5610. https://doi.org/10.1021/cr400131u

Inamdar, A., Pote, S., Sawant, S., Salve, P. S., Suryawanshi, S. S., & Palled, M. (2023). *Physicochemical and pharmacokinetic properties' screening of selected cardiovascular agents: An in-silico approach*. https://doi.org/10.21203/rs.3.rs-2653667/v1

Jain, A. K., Sharma, S., Vaidya, A., Ravichandran, V., & Agrawal, R. K. (2013). 1, 3, 4-Thiadiazole and its derivatives: A review on recent progress in biological activities. *Chemical Biology & Drug Design, 81*(5), 557–576. https://doi.org/10.1111/cbdd.12125

Kaya, B., Acar Çevik, U., Çiftçi, B., Duran, H. E., Türkeş, C., Işık, M., ... & Beydemir, S. (2024). Synthesis, α-glucosidase, α-amylase, and aldol reductase inhibitory activity with molecular docking study of novel imidazo [1, 2-a] pyridine derivatives. *ACS Omega, 9*(42), 42905–42914. https://doi.org/10.1021/acsomega.4c05619

Kaya, B., Acar Çevik, U., Necip, A., Duran, H. E., Çiftçi, B., Işık, M., ... & Beydemir, S. (2025). Design, synthesis, biological evaluation, and molecular docking studies of novel 1, 3, 4-Thiadiazole derivatives targeting both aldose reductase and α-Glucosidase for diabetes mellitus. *ACS Omega, 10*(18), 18812–18828. https://doi.org/10.1021/acsomega.5c00566

Matysiak, J. (2015). Biological and pharmacological activities of 1, 3, 4-thiadiazole based compounds. *Mini Reviews in Medicinal Chemistry, 15*(9), 762–775. https://doi.org/10.2174/1389557515666150519104057

Patel, P., Shah, D., Bambharoliya, T., Patel, V., Patel, M., Patel, D., ... & Patel, A. (2024). A review on the development of novel heterocycles as α-glucosidase inhibitors for the treatment of type-2 diabetes mellitus. *Medicinal Chemistry, 20*(5), 503–536. https://doi.org/10.2174/0115734064264591231031065639

Polya, G., & Read, R. C. (2012). *Combinatorial enumeration of groups, graphs, and chemical compounds*. Springer Science & Business Media. https://doi.org/10.1007/978-1-4612-4664-0

Sharma, R., Roy, S., & Kumar, A. (2025). Drug repurposing and virtual screening. In *Advances in Pharmaceutical Product Development* (pp. 399–421). Springer Nature Singapore. https://doi.org/10.1007/978-981-97-9230-6_16

Shen, X., Saburi, W., Gai, Z., Kato, K., Ojima-Kato, T., Yu, J., ... & Yao, M. (2015). Structural analysis of the α-glucosidase HaG provides new insights into substrate specificity and catalytic mechanism. *Biological Crystallography, 71*(6), 1382–1391. https://doi.org/10.1107/S139900471500721X

Shulgau, Z., Palamarchuk, I. V., Sergazy, S., Urazbayeva, A., Ramankulov, Y., & Kulakov, I. V. (2024). Synthesis, computational study, and in vitro α-Glucosidase inhibitory action of 1, 3, 4-Thiadiazole derivatives of 3-Aminopyridin-2 (1 H)-ones. *Pharmaceuticals, 17*(3), 377. https://doi.org/10.3390/ph17030377

Singh, Y., Jaswal, S., Singh, S., Verma, S. K., & Thareja, S. (2022). Dual aromatase-steroid sulfatase inhibitors (DASI's) for the treatment of breast cancer: A structure guided ligand based designing approach. *Journal of Biomolecular Structure* & *Dynamics, 41*(20), 10604–10626. https://doi.org/10.1080/07391102.2022.2155702

Stitou, M., Toufik, H., Bouachrine, M., & Lamchouri, F. (2021). Quantitative structure–activity relationships analysis, homology modeling, docking and molecular dynamics studies of triterpenoid saponins as Kirsten rat sarcoma inhibitors. *Journal of Biomolecular Structure and Dynamics, 39*(1), 152–170. https://doi.org/10.1080/07391102.2019.1707122

Uddin, J., Ullah, S., Halim, S. A., Waqas, M., Ibrar, A., Khan, I., ... & Al-Harrasi, A. (2023). Triazolothiadiazoles and triazolothiadiazines as new and potent urease inhibitors: Insights from in vitro assay, kinetics data, and in silico assessment. *ACS Omega, 8*(35), 31890–31898. https://doi.org/10.1021/acsomega.3c03546

Van de Laar, F. A., Lucassen, P. L., Akkermans, R. P., Van de Lisdonk, E. H., Rutten, G. E., & Van Weel, C. (2005). α-Glucosidase inhibitors for patients with type 2 diabetes: Results from a Cochrane systematic review and meta-analysis. *Diabetes Care, 28*(1), 154–163. https://doi.org/10.2337/diacare.28.1.154

Vanajothi, R., Hemamalini, V., Jeyakanthan, J., & Premkumar, K. (2020). Ligand-based pharmacophore mapping and virtual screening for identification of potential discoidin domain receptor 1 inhibitors. *Journal of Biomolecular Structure* & *Dynamics, 38*(9), 2800–2808. https://doi.org/10.1080/07391102.2019.1640132

Veerasamy, R., Rajak, H., Jain, A., Sivadasan, S., Varghese, C. P., & Agrawal, R. K. (2011). Validation of QSAR models-strategies and importance. *Int. J. Drug Des. Discov, 3*, 511–519. https://doi.org/10.37285/ijddd.2.3.1

Verma, S. K., Kumar, N., & Thareja, S. (2021). Gaussian field-based comparative 3D QSAR modelling for the identification of favourable pharmacophoric features of chromene derivatives as selective inhibitors of ALR2 over ALR1. *Structural Chemistry, 32*(3), 1289–1298. https://doi.org/10.1007/s11224-020-01714-6

Vishwakarma, K., & Bhatt, H. (2021). Molecular modelling of quinoline derivatives as telomerase inhibitors through 3D-QSAR, molecular dynamics simulation, and molecular docking techniques. *Journal of Molecular Modeling, 27*(2), 30. https://doi.org/10.1007/s00894-020-04648-2

Yadav, R., Imran, M., Dhamija, P., Chaurasia, D. K., & Handu, S. (2021). Virtual screening, ADMET prediction and dynamics simulation of potential compounds targeting the main protease of SARS-CoV-2. *Journal of Biomolecular Structure and Dynamics, 39*(17), 6617–6632. https://doi.org/10.1080/07391102.2020.1796812